Integrated Master in Biomedical Engineering

Faculty of Sciences and Technology

University of Coimbra

BroadBand Excitation for Bioelectrical Impedance Spectroscopy

A Comparative Study

Mariana Sequeira

2012

Integrated Master in Biomedical Engineering

Faculty of Sciences and Technology

University of Coimbra

BroadBand Excitation for Bioelectrical Impedance Spectroscopy

A Comparative Study

Dissertação apresentada à Universidade de Coimbra para cumprimento dos requisitos necessários à obtenção do grau de Mestre em Engenharia Biomédica, realizada sobe a orientação Professor Doutor Carlos Correia, Grupo de Electrónica e Instrumentação da Universidade de Coimbra e do Doutor João Cardoso, Grupo de Electrónica e Instrumentação da Universidade de Coimbra.

Mariana Sequeira

2012

This work is funded by FEDER trough the *Programa Operacional Factores de Competividade* – COMPETE and by National funds through FCT – *Fundação para a Ciência e Tecnologia* in the frame of *Centro de Instrumentação – Unidade* 217.

"Success is a science; if you have the conditions, you get the results"

Oscar Wilde

"Once we accept our limits, we go beyond then"

Albert Einstein

"Quem quis, sempre pôde"

Luiz Vaz de Camões

Contents

List of Figures

List of Tables

Acronyms

AC	Alternating Current
ADC	Analog to Digital Converter
CPE	Constant Phase Element
CS	Current Sources
DC	Direct Current
DTFT	Discrete Time Fourier Transform
EIS	Electrical Impedance Spectroscopy
FFT	Fast Fourier Transform
FRA	Frequency Response Analyzer
PSD	Phase Sensitive Detection
SNR	Signal to Noise Ratio
THD	Total Harmonic Distortion
USB	Universal Serial Bus
VS	Voltage Source

List of Original Papers

Parts of this thesis have been published in the following papers:

I. *Bioimpedance parameters as a risk factor to asses pine decay. An innovative approach to the diagnosis of plant diseases.* E. Borges, M. Sequeira, André F. V. Cortez, H. Catarina Pereira, T. Pereira, V. Almeida, T. M. Vasconcelos, I. M. Duarte, N. Nazaré, J. Cardoso and C. Correia. 2012. Submitted to Biostec – Biosignals (The Internacional Joint Conference on Biomedical Engineering Systems and Technologies), 11-14 Feb. 2013, Barcelona, 12pp.

II. *Design and Evaluation of a Portable Electrical Impedance Spectroscopy System – An Innovative Application for the Diagnosis of Plant Disease.* E. Borges, M. Sequeira, André F. V. Cortez, H. Catarina Pereira, T. Pereira, V. Almeida, J. Cardoso, C. Correia, T. M. Vasconcelos, I. M. Duarte, N. Nazaré, J. Cardoso and C. Correia. 2012.

III. *An essential overview on EIS and related issues.* E. Borges, M. Sequeira, H. Catarina Pereira, T. Pereira, V. Almeida, J. Cardoso and C. Correia. 2012.

The first paper proposed a portable EIS system for biological applications and a biological study for discrimination between physiological states of pines trees.
The second and third have not yet undergone since the provisional patent prevented a timely submission.

The provisional patent was submitted to INPI (*Instituto Nacional de Propriedade Industrial)* during this project with the title: "System to assess physiological states of plant tissues*, in vivo* and/or *in situ*, using impedance techniques." March 2012.

Acknowledgements

I would like to thank my supervisors, Prof. Dr. Carlos Correia and PhD João Cardoso, for their support and aid along all this work. I am very gratefulness to Prof. Dr. Carlos Correia for his patience, guidance and for incentivized me to appreciate the world of research.

I also would like to thank Professor Jorge Canhoto and MsC Lara Currais from *Centro de Ecologia Funcional* of University of Coimbra for the support and knowledge, as well as the Quinvita enterprise for kindly sharing *Jatropha curcas* seeds and trees used in this project.

I would like to express my especial gratitude to MsC Elisabeth Borges who was a guide to me, giving continuous and sincere help and who always believed in my capabilities throughout the project work.

I must thank all the members of the GEI for the good work environment, especially to MsC Vânia Almeida, Pedro Santos and Pedro Vaz who were always ready to helping and advising me.

Thanks to all my friends that even though indirectly helped in the development of this project.

I must especially thank Gabriel Campos who always supported and encouraged me even when I did not believe that would be able to finish this work.

And finally, to my family but especially to my dear parents, for being my safe haven, for you were the best parents that anyone can have. To my brother, thank you for always encouraging me and for pride shown in each of my conquests. To them I dedicate this work.

Abstract

Electrical Impedance Spectroscopy, EIS, has been proving efficacy and utility in a wide range of areas, from the characterization of biological tissues to living organisms.

Typical equipments are expensive, unfeasible for *in vivo* and in field applications and unspecific for a concrete application. Herein is proposed a portable EIS system for several biological applications, as the discrimination between different physiological states, species cultivars or environmental conditions.

The nature of the impedance excitation signal varies depending on the application. The frequency limits and the type of the excitation signal also depend on the object under study. Whereupon, the discussion on what type of excitation waveform is the most convenient, remains. This context has been the main motivation for the work presented. This project was centered on finding the more effective broadband signal to perform impedance measurements as a function of time.

Biological tests using the proposed EIS system were performed and quite good results were achieved. The results showed a direct relationship between the water content and impedance values. The technique allowed the monitoring of pine decay, the discrimination between healthy and unhealthy plants and the segregation of different Jatropha seeds.

The experimental hardware and several simulations showed that broadband signals have many drawbacks, but improves the hardware can reveal its advantages, such as the fast, and consequently accurate, bioimpedance measurements.

Keywords: Electrical Impedance Spectroscopy, Bioimpedance, Biological Applications, Broadband Signals, Waveform, Plant Diseases, Physiological States.

Resumo

A Espectroscopia de Impedância Elétrica tem provado a sua eficácia e utilidade numa vasta gama de áreas, desde a caracterização de tecidos biológicos aos organismos vivos. Os equipamentos disponíveis são caros, de difícil utilização *in vivo* e no campo e pouco específicos na sua aplicação. Assim é proposto um sistema portátil para diferentes aplicações como a distinção entre diferentes estados fisiológicos, elementos da mesma espécie e diferentes condições ambientais.

A natureza do sinal de excitação pode variar de acordo com a aplicação. Os limites de frequência e o tipo do sinal também dependem do objeto de estudo. Desta forma mantém-se a discussão sobre o tipo de forma de onda mais adequado. Estes fatores foram a principal motivação para o trabalho apresentado. O projeto esteve centrado em encontrar um sinal de banda larga eficaz para a realização de medições de impedância no domínio do tempo.

Alguns testes biológicos usando o sistema de espectroscopia foram realizados com a obtenção de bons resultados. Os resultados apresentados permitiram estabelecer uma relação direta entre o conteúdo em água e os valores de impedância. A técnica permitiu também a distinção entre plantas saudáveis e doentes bem como a separação entre diferentes sementes de Jatropha.

O *hardware* experimental e as simulações mostraram que os sinais propostos têm muitos inconvenientes, mas uma melhoria do hardware pode revelar as suas vantagens, como a capacidade de medir rápidas variações de bioimpedânica.

Palavras-chave: Espectroscopia de Impedância Elétrica, Bioimpedânica, Aplicações biológicas, Sinais de Banda Larga, Estados Fisiológicos, Doenças Vegetais.

Chapter 1

Introduction

1.1 Motivation

There are several plant diseases affecting different cultures of huge economic importance, such as chestnuts, pines and vineyard. Most of them are promoted by biological agents such as fungus, virus, nematodes and cause tress stress and mortality with fast and asymptomatic spread. The standard method to diagnose diseases is the symptomatology visualization by a skilled person. Although, the external symptoms are only visible during the terminal stages the physiological states of the plant tissues alter in earlier stages. Additionally, some alterations may not imply any disease. So, because of the fact that the symptoms are imperceptible from the outside and there is still no cure the solution passes through cut trees of a given area and burned the infected material. The result of this action is the deforestation because not only the diseased plant is cut but also the neighboring plants.

In addition to the standard method there are some techniques of analysis performed in the laboratory, such as the spectroscopy analysis of the monoterpenes. This technique involves sample collection, reagents are necessary to perform the analysis, it is time-consuming and expensive. Some biosensors may also be used for measure an amount of a specific compound in a plant product that may indicate some specific condition of its.

An alternative of those methods is the Electric Impedance Spectroscopy technique as a solution for diagnosing plant diseases and a method to asses changes in

physiological states of plant tissues. Explore the potential of this alternative method was one of the objectives of this work.

1.2 Main Contributions

The principle aim of the work describe here is the study of the possibility of using a different excitation signal for electrical impedance measurement. Since the use of a chirp pulse (sweep of frequencies) is successfully tested. The idea is to use a broadband excitation signal to cover the frequency range of interest, according the biological application, and compare the results from the two different techniques. This work is a continuity project once the Electric Impedance Spectroscopy system had already been developed in the research group and different biological tests were performed to prove the usefulness of the developed system.

1.3 Project Research Team

This work was developed at Group of Electronics and Instrumentation (GEI), integrating part of the Instrumentation Center (CI) of the Physics Department of the University of Coimbra, in the framework of partnership with Escola Superior Agrária de Coimbra, ESAC, the enterprise Exatronic – Innovation Insight, and the Botanic Department of the University of Coimbra. It is inserted on a PhD project in the research field of Bioimpedance. The persons involved in the above project as well as their areas of contribution, are summarized in the following table.

Table 1.1: Team Members of the project and its contribution.

Team Member	Main Contribution	Institution
Prof. Dr. Carlos Correia	Scientific Supervisor	GEI-UC
Doctor João Cardoso	Technical Supervisor	
MSc Elisabeth Ferreira	PhD Student	
Prof. Dr. Teresa Vasconcelos	Scientific Supervisor	CERNAS-ESAC
Prof. Dr. Isabel Duarte	Scientific Supervisor	
Eng. Neuza Nazaré	Technical Supervisor	
Prof. Dr. Jorge Canhoto	Scientific Supervisor	CEF-UC
MSc Lara Currais	PhD Student	
Eng. Nuno Gomes	Technical Supervisor	Exatronic
Mariana Sequeira	Biomedical Engineering Project Student	GEI-UC
André Cortez	Physics Engineering Project Student	

1.4 Overview of the dissertation

In order to guide the reading throughout the dissertation a brief summary of the contents of each chapter is presented:

- Chapter 2 – *Theoretical Background*: theoretical concepts about impedance and related concepts with the studied of impedance in the application field are explored;
- Chapter 3 – *EIS System*: description of the developed hardware and software and presentation of performing tests results;

- Chapter 4 – *Broadband Signals Simulation:* simulations results are shown and discussed;
- Chapter 5 – *Hardware – Experimental Setups:* experimental setups for broadband excitation are presented and the results discussed;
- Chapter 6 – *Biological application tests:* results from different biological application are shown and discussed;
- Chapter 7 – *Conclusion and Future Work:* some conclusions are drawn that summarized the most important contribution of this work. The developments foreseen in a near future are also mentioned.

Chapter 2

Theoretical Background

This chapter begins with an overview of the principles of Electrical Impedance Spectroscopy and its application fields. Afterwards, a discussion of used biological models, methods to asses impedance and the nature of excitation signal is pursued. The last section gives a brief overview of commercial devices used impedance spectroscopy.

2.1 Principles of Electrical Impedance Spectroscopy

The concept of impedance was introduced by Oliver Heaviside in the 1880 and after developed in terms of vector diagrams and complex representation by C. P. Steinmetz [1]. This concept has become a fundamental concept in electrical engineering. The electrical impedance is defined as the relation between the input voltage and the input current at a certain frequency. So, the current I, as it passes across a section of a material of impedance Z, drops the voltage V, established between two given points of the same section, yielding the well-known generalized Ohm's law:

$$V = I.Z \tag{2.1}$$

If V and I complex numbers also Z is a complex number with the magnitude equal to the relation of magnitudes and phase equal to the difference of phases. Than the Ohm´s law can be rewritten (as equation **2.2** expresses), since the current flow lag the voltage by a phase of θ.

$$V = I|Z|e^{j\theta} \tag{2.2}$$

The impedance can be divided into resistance which is the real part and it is responsible for the power loss while the imaginary part is called reactance and causes the delay between voltage and current [2]. So, as a complex quantity it can be expressed as:

$$Z = R + jX \tag{2.3}$$

Where Z is the impedance value, j is the complex number and R and X are the resistance and reactance, respectively. It is common the impedance representation on a vector plane, such as that shown on Figure 2.1.

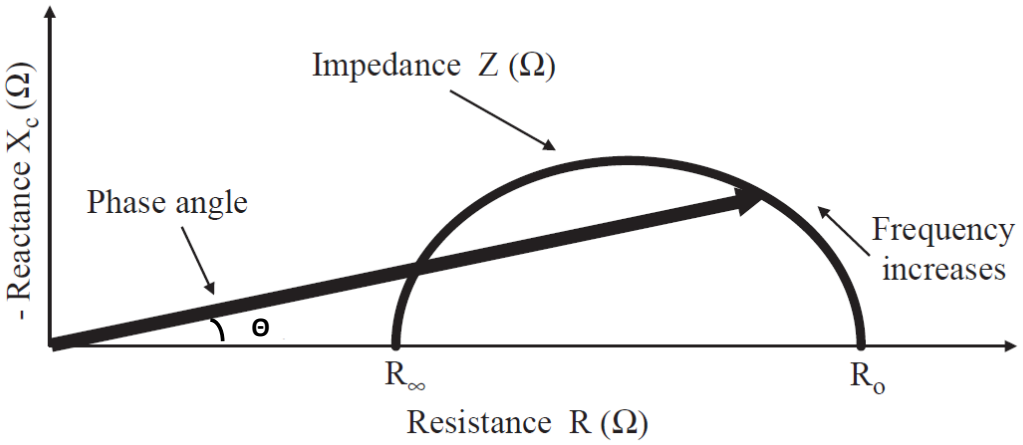

Figure 2.1: A schematic diagram of a typical impedance complex locus. Adapted from [3].

This representation has the particularity to plot the negative of the imaginary part of the impedance against the real part and is called Cole-Cole plot or Cole diagram. This sign convention has been adapted in order to have the diagram plotted in the first quadrant of the complex plane [4]. The choice was based on the impedance measurements over high frequency range that only exhibit capacitive behavior [4].

One of the most studied and implemented technique, based on the electrical impedance concept, is the Electrical Impedance Spectroscopy, EIS. This technique allows the assessment of the impedance spectrum (i.e. impedance values for a range of frequencies) of a sample, which evidently contains more information than a single frequency impedance measurement.

EIS is a method for studying the properties and structure of organic and inorganic materials [5]. The measurements can be performed in a wide frequency range and allows the characterization of solids, liquids and suspensions [6]. The information is achieved by driving an alternating current (AC) into the sample and recording the changes in the amplitude and phase of the applied AC signal [7]. This method has proved its value in the characterization of living tissues and fluids [8]. Concerning the vegetable field the application of this technique has been used in the quality control processes of fruits and vegetables, as well as in the monitoring the influence of temperature or other external agents in the physiological state of living plants [9, 10]. In these cases, the electrical impedance of a biological material, or simply bioimpedance, is defined as a passive electrical property that measures the opposition of a given material, relatively to an alternating current flow, applied by an external electric field. As already mentioned, the impedance of the sample is represented by means of the relationship between the resistance versus reactance and these two features express the electrical properties of the material under investigation.

The impedance of a vegetal tissue represents an electrical characteristic determined by the structure and composition of cellular tissues, so the cell membranes, intracellular fluid (cytosol) and extracellular fluid are the major contributors of the impedance of biological tissues [3]. The portion of current passing through the cell depends in the AC frequency and tissue properties.

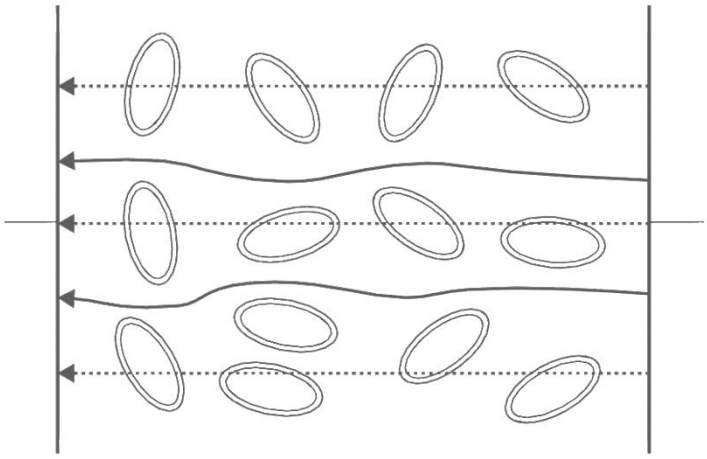

Figure 2.2: Pathway of current at different frequencies: low frequencies (continuous line) and high frequencies (dashed line). Adapted from [11].

For low frequency AC signals the current flows only through the extracellular medium [12]. On the other hand, using high frequency AC signals allows the increasing of current passing through the cytosol [12] (see Figure 2.2). So, the cell membrane impedance decreases with increasing frequency [5].

Because of this dependence different properties can be examined and quantified in EIS by the analysis of the equivalent electric circuit. So, with a proper electrical model it is possible to study the effects of diverse factors on tissue properties, according to changes in the model parameters [13].

The electrical properties reflect the tissue integrity and large changes in impedance can allow the determination of the influence of temperature, water content, hydric stress or humidity. Many studies for different authors were performed for understand the impedance changes. *Vozáry et al.* [14] had proved that both magnitude and phase angle of impedance were decreased as the deformation or stress increased. These changes can be explained by changes in intracellular and intercellular part under stress. The integrity of the cell membrane is affected by the temperature so that effect is also reflected in dielectric properties of tissues. *Dejmek et al.* [9] concluded that the electrical impedance decreased after heating or freezing process

because the plasma membrane was damaged [9] . Finally, also the water content of the tissue may be interfering with impedance values. Processes of dehydration and dilutions proved the influence of this parameter where the values of impedance are proportional to the water content of the sample [15].

In the other way, the impedance values are not only dependents by the electrical properties of the material but also by the geometrical constrains.

2.2 Biological Models

The cytosol and the extracellular fluid are mostly constituted by water, consist in electrolytes, and act like ohmic resistors, while the insulating membranes behave like capacitors [3]. It is, therefore, possible to depict the behavior of a biological tissue by the representation of capacitive and resistive elements of a respective equivalent electrical circuit. The equivalent circuit models are important because they are useful to attribute a physical meaning to the impedance parameters. However, the problem of an electrical model of the physical or chemical process in tissue is that it is impossible to mimic the real electrical behavior with only physical realizable components [16].

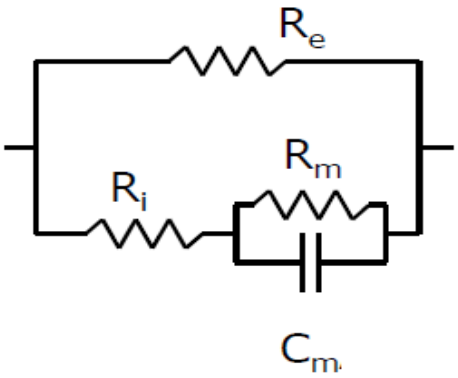

Figure 2.3: Equivalent circuit model. R_i: resistance of the intracellular electrolytic medium; R_e: resistance of the extracellular electrolytic medium; R_m: resistance of cell membrane; C_m: capacitance of cell membrane.

One of the first electrical models for the electrical properties of living tissues was proposed for Lapicque (1907) to model the excitation of nerve membrane [4]. The 'three-component' model consists of a parallel combination of a resistance and a capacitor, in series with another resistance (Figure 2.4). However, the most successful electrical model was introduced for Frick and Morse (1925) and it consists of a resistance in parallel with the series of a resistance and a capacitor (Figure 2.4) [4]. This equivalent circuit was developed based on measurements on suspensions of red blood cells at various frequencies [4]. The Frick and Morse model has been extensively used because of its simplicity and it is able to describe qualitatively the observed in the experimental results. The Lapicque model ignoring any current flow around and between the cells, so the two models can figure together (Figure 2.3). The equivalent model at Figure 2.3 can be simplified into the Frick and Morse model, once the membrane conductance is very low the membrane resistance can be ignored [2]. Although, the previous model is very simple and a biological tissue tends to be more complex than that.

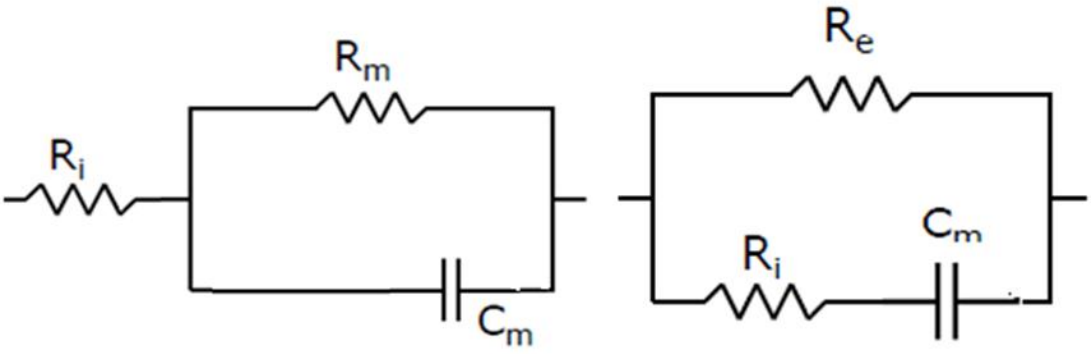

Figure 2.4: Lapicque Model (left) and Frick and Morse Model (right). R_i: resistance of intracellular electrolytic medium; R_m: resistance of cell membrane; R_i: resistance of the extracellular electrolytic medium; C_m: capacitance of cell membrane.

The capacitive model proposed by Frick and Morse was not accurate enough to fit the experimental data in biological tissues. Plot the imaginary part versus real part of the impedance measurements produces a semicircle with the center depleted in the

reference to the real axis (see Figure 2.5). This behavior is common to all biological tissues, although the depletion is tissue-dependent. This fact suggests that the models presented do not reflect the behavior of biological tissues entirely [17].

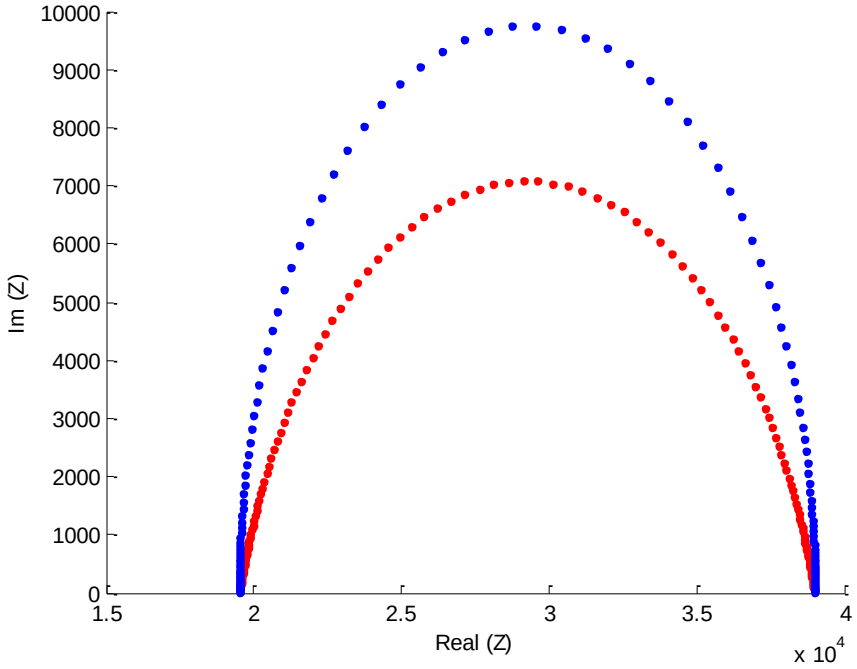

Figure 2.5: Cole-Cole plot: generated by Cole equation parameters (blue) and impedance data of a biological sample (red).

The solution was proposed by Cole (1932) who noted that many cell membranes could be represented by the series combination of a frequency dependent capacitor and resistance [17]. So, Cole included a Constant Phase Element (CPE) in replacement of the ideal capacitor and was the first to use an equivalent circuit model which involves the combination of a CPE and a resistance [18]. The combination of these elements may be in series or in parallel and the choice will depend on the system under investigation. Moreover, much of the literature has used a resistance in series with a CPE (see Figure 2.6).

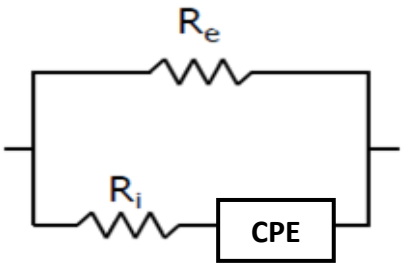

Figure 2.6: Cole Model. R_e: extra-cellular electrolytic medium; R_i: intra-cellular electrolytic medium; CPE: constant-phase element.

Cole also introduced (1940) a mathematical expression able to describe the impedance of a biological tissue and the behavior observed experimentally ('depressed semicircles') [here expressed as in [2]]:

$$Z = Z_\infty + \frac{\Delta R}{1 + (j\omega\tau)^\alpha}, \qquad \Delta R = R_0 - R_\infty \tag{2.4}$$

Where Z is the impedance value at frequency ω, Z_∞ is the impedance at infinite frequency, j is the complex number, R_0 is the impedance at zero frequency, τ is the characteristic time constant and α is a dimensionless parameter with a value between 0 and 1 [2].

The α value can be regarded as parameter denoting the derivation from Frick-Morse model, because the Cole equation and the Frick-Morse equivalent model only produced the same Cole plot if $\alpha = 1$ [19].

Although, CPE is a non-physical element its mathematical expression is very simple (here expressed as in [19]) and allows the simulation of its behavior and notice that the fitting of experimental data is perfect whatever the value of α [20].

$$Z_{CPE} = \frac{K}{(jw)^\alpha}, \qquad K = \frac{\Delta R}{\tau^\alpha} \tag{2.5}$$

The α parameter is often ignored in favour of other bioimpedance parameters but has been demonstrated its application to the characterization of living tissues because it is closely related with the extra-cellular space morphology and dimensions [19].

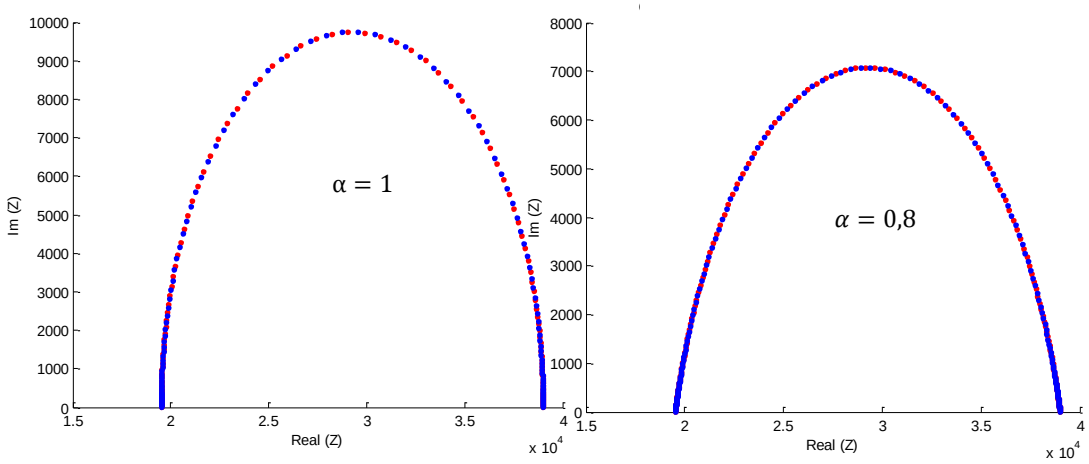

Figure 2.7: Cole-Cole Plots. Fitting impedance data with different α values

2.3 Methods to Asses Impedance

Impedance is defined in the frequency domain but it can be measured in both the frequency and time domains. Frequency domain impedance measurements are carried out using a sinusoidal excitation with frequency as the independent variable, although in time domain the time is the independent variable and the impedance as a function of frequency can be extracted by time-to-frequency conversion techniques [21]. Generally, the time domain methods use digital processing techniques while the frequency domain methods use analog techniques [1].

2.3.1 Frequency Domain Methods

The most common approach in assessing passive electrical properties is performed a frequency sweep with phase sensitive current and voltage measurement at each frequency. Due to the time requirements this method is not suited for recovering fast impedance changes on biological samples [22]. So, the excitation and monitoring the response as a function of time will reduce the measurement time.

There are many measurement methods in frequency domain to choose, which has advantages and disadvantages. The choice must consider such factors as frequency coverage, measurement range and measurement accuracy [23]. As an indirect method, a variety of bridges have been used for impedance measurement. Their main advantage is their high resolution which is a very important feature for extending dielectric measurements to low frequencies in tissue [1]. Automated bridges are preferred to manual bridges and they have given way to other methods for bioimpedance measurements, such as lock-in amplifiers [11].

Direct measurements can be used to acquire impedance data more rapidly than bridges methods. Oscilloscopic methods using a twin-beam oscilloscope for recording the voltage drop across a series resistance. The magnitude of the impedance can be calculated from the ratio of the two peak-to-peak voltages, according to the following equation:

$$|Z| = \frac{R_s|e(jw)|}{|e_R(jw)|} \tag{2.6}$$

Where R_s is the series resistance, $e(jw)$ and $e_R(jw)$ are the oscilloscope traces that results from the imposition of a sine wave between the working and reference electrodes, as Figure 2.8 depicts.

The phase angle can be directly observed from the oscilloscope.

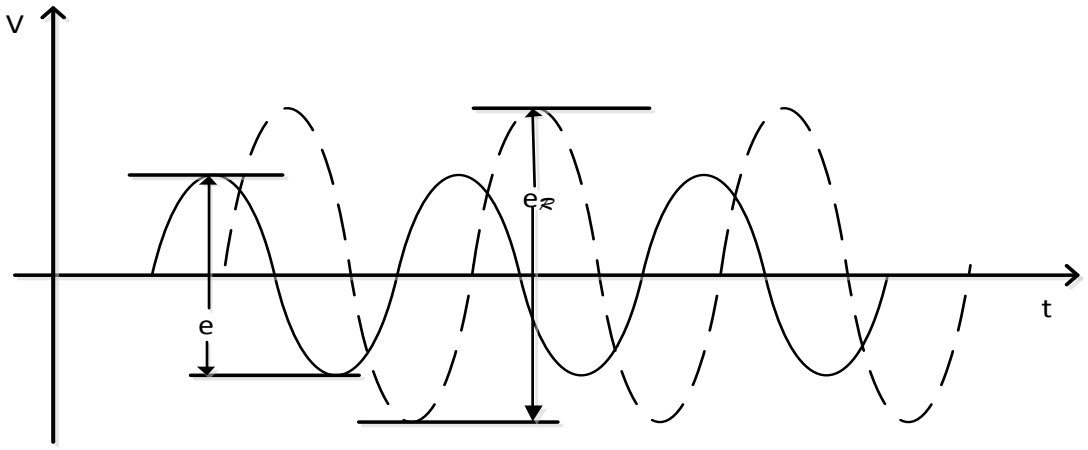

Figure 2.8: Direct measurement of impedance using a twin-beam oscilloscope. Adapted from [1].

The primary limitation of this technique is precision, the linearity is seldom better than 1% and it is difficult to measure phase angle with a precision better than 2° [24].

It is possible to use automated Frequency Response Analysis (FRA) for determine the impedance by correlating the object response with two synchronous reference signals, one of which is in phase with the sine-wave and the other shift 90° in phase (see Figure 2.9) [1]. FRAs have high-precision and are very convenient method for impedance measurements in electrochemical systems; however the cost is the main disadvantage [1]. Additionally, automated impedance analyzers and spectrum analyzers are used methods. The first has the advantages of high speed, high precision and usable up to very high frequencies [1]. While the spectrum analyzer can be used to measure impedances at audio and higher frequencies, using a variety of input excitation functions [1].

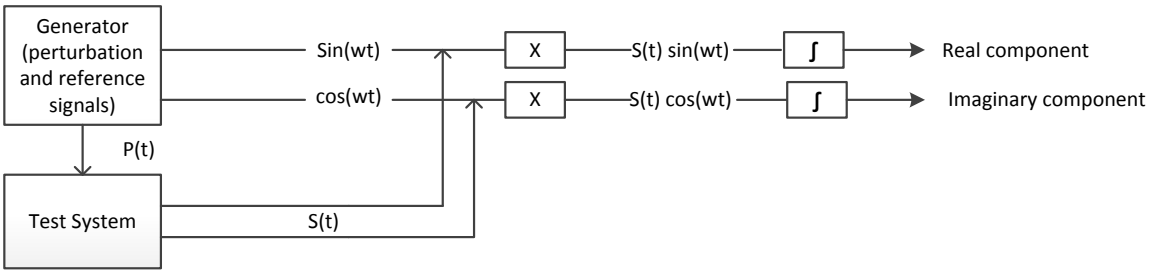

Figure 2.9: Schematic of a typical FRA. Adapted from [1].

The use of Kramers-Kronig transforms is a simple method of obtaining complex impedance spectra using one or two AC multimeters. This method is very simple, low cost and can operate to very high frequencies, although the practical limitation is imposed at low frequencies [1].

2.3.2 Time Domain Methods

The measurement principle in time domain involves the application of a broad bandwidth signal to the object and measuring the answer as function of time. The applied signal and the response are transformed into frequency domain where the magnitude and phase can be calculated. To convert data collected from time domain into the frequency domain several integral transforms can be used, including the Discrete Time Fourier Transform (DTFT), the Fast Fourier Transform (FFT) and the Laplace Transform [10, 25]. Any of these techniques required two stages of data manipulation to obtain the impedance as a function of frequency. So, the input and output functions must be sampled and recorded in the time window of interest and then the transform of each must be computed [26].

Time domain measurements need fast analog-digital converter, ADC, and enough data points to reconstruct the input-output frequency response [21]. So, the sampling rate, the resolution of the ADC as well as the noise level of the amplifiers are the most important quality parameters of the equipment [27]. The FFT method removes the necessity of a phase sensitive detector, allows a faster measurement and impedance data at many different frequencies can be obtained simultaneously [25]. Time domain based measurements is the option to compensate parasitic reflections and transmission losses at specific parts of the measurement arrangement, as connectors or cables [16].

2.4 Excitation Signal

2.4.1 Nature

The discussion on what is the most convenient nature of the excitation signal still remains. So, the EIS can be performed by applying current through the electrodes and measuring the voltage and also by applying voltage and measuring the current. Even current or voltage may be applied on the surface of the sample some authors have shown that the precision of current excitation is a critical limitation to measurements. [28]. Current sources, CS, are limited in their precision by their output impedance because its changes at higher frequencies due to the capacitive components of the sources [28]. So, CS accuracy decreases at high frequencies [29]. Additionally, this kind of sources tends to have limited bandwidth and requires a large number of high-precision components [30]. However, CS provide suitable controlled means of current injection [31] and present reduced noise due to spatial variation when compared with voltage sources, VS [32].

In order to improve the performance at high frequencies the literature suggests a method based on a voltage source. VS, although producing less optimal EIS system, can operate over a sufficient broad frequency range [29, 30] and are generally easier and less costly to implemented, because they are built with less expensive components [30].

2.4.2 Type

Sine wave excitation and phase-sensitive demodulation are common tools for impedance measurement in biological application [33]. A sine wave pulse with linearly increasing angular frequency (sweep pulse) is the most commonly used signal. However, the sweep of a frequency range is not a good choice for recovering fast impedance changes that may be occur in the samples. Additionally, the bioimpedance measurement requires the signal generation which means significant energy consumption [34]. So, is important to use a minimal-energy excitation signal where the desired broad spectrum

can be measured[35]. Both multiple sine-wave perturbation and time domain can perform fast bioimpedance measurements [36]. Although, the method using multiple sine-wave can obtained simultaneously impedance data at different frequencies a complex signal generator and large memory are inevitable [25]. So, the alternative for excitation is a broadband signal such as a rectangular wave pulse, Gaussian function and its derivatives and also Sinc signals and its modifications. The usage of the rectangular wave pulse is simple but not always the best choice because the distribution of spectral energy is not adjustable, meaning that energy is wasted in frequency regions without interest [34]. Therefore is important to find more effective waveforms for excitation pulses with the frequency range of interest and an appropriate sampling rate. In these cases the impedance measurements and the response signal are performed as a function of time and converted to frequency domain by means of FFT.

Table 2.1: Excitation pulses with different waveforms: advantages and drawbacks.

Pulse Type	Waveform	Advantages	Disadvantages
Step	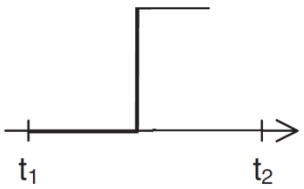	• Easier to obtain; • Wide frequency range using DTFT.	• Low-level noise significantly disturbs the impedance spectra.
Rectangular	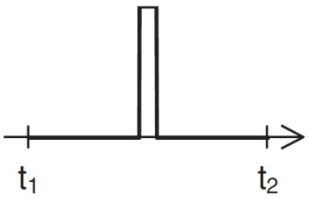	• Quick method; • Fast changes of the object impedance can be monitored.	• The distribution of spectral energy is not adjustable[1].

[1] Energy is wasted in frequency regions without interest.

Table 2.2: Excitation pulses with different waveforms: advantages and drawbacks. (cont.)

Pulse Type	Waveform	Advantages	Disadvantages
Gaussian	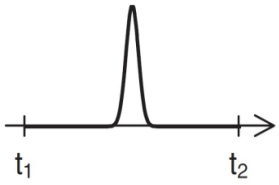	• Higher energy density within the desired range of the spectrum.	
Sinc		• Preferred for biological applications; • A difference of two $\sin(wt)$ pulses enables to shift the excitation bandwidth to the desired higher frequency range.	• Signal waveform is more complex.
Chirp	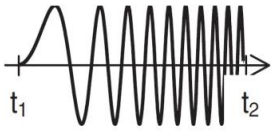	• The most informative; • Low crest-factor[2].	• Windowing problems; • Long excitation periods.

Every excitation type of signals has advantages and drawbacks (Table 2.1 and Table 2.2). The Gaussian function and its derivatives are simple but they do not always perform optimally [27]. To cover a desired frequency range with a Gaussian pulse, two sequential pulses must be applied and the FFT performed for both, in order to obtain the impedance spectrum [22]. The main disadvantage is that all excitation energy cannot be in the bandwidth of interest.

[2] Crest factor, is a measurement of a waveform, calculated from the peak amplitude of the waveform divided by the RMS value of the waveform

Although, the Sinc function has a complex waveform it has a good flat spectrum [37]. To obtain a desired higher frequency range a difference of two Sinc pulses can be performed [34]. Therefore, the Haversinc pulse and the first derivative of the Gaussian function are preferred for biological application [35]. Finally, depending on the object under investigation different excitation waveforms can be matched, and this is the main advantage of arbitrary waveform generation [22].

2.5 State of Art

There are several different kinds of automated instruments for impedance measurements, which, generally, can be divided into two categories: LCR-meters and impedance analyzers. LCR-meters use the auto-balancing bridge technique to measure impedance of materials. They can generally be used in a frequency range roughly between 5 Hz and 1 GHz [11]. Low cost meters are also available, like the SR 720 or HP 4263 B which measure at five pre-defined frequencies from 100 Hz to 100 kHz [11]. Additionally, instruments as NPS 1890 have the limitation of not operate at arbitrary frequency and therefore unable to produce an impedance spectrum.

Impedance analyzers are also called frequency response analyzers and are in most cases combined instruments employing different techniques to cover a larger frequency range. Although, Solartron 1650 and HP 4194A are the most cited in the literature, these instruments are not portable and very expensive (higher than 40.000€) [38, 39].

The Agilent Technologies 4294A precision impedance analyzer is an integrated solution for efficient impedance measurement and analysis of electronics devices as well as non-electronic material [40]. This system accurate measurement over wide impedance range and wide frequency range (40 Hz to 110 MHz) with the basic impedance accuracy of +/- 0, 08% [38]. The Agilent 4294A has powerful impedance analysis functions and is easy to use and has versatile PC connectivity [38].

The main application field is in electronic devices but some materials as dielectric, magnetic and semiconductor materials could be analyzed. This system has an equivalent

circuit function that enables modeling of the impedance vs. frequency characteristics with three or four elements. This feature is used to fit the measured data or to simulate the material impedance based on the value of each circuit model element [38].

Solarton analytical has a 1260 Impedance/gain-Phase Analyzer (1260 FRA) which uses digital correlation techniques for measurements in the range 10 µHz to 32 MHz [39].

This system was produced to provide cost effective solutions for DC and AC analysis and offers an outstanding measurement for impedance spectroscopy. The ADCs used have a resolution of 16 bits and the basic accuracy is 0.1% for magnitude and 0.1° for phase measurements [16, 39]. It has 2-, 3- and 4-terminal measurement configuration and a software package to simplify experiments and optimized throughput. Additionally, it can be used to measure highly conducting materials with 4 electrodes configuration as well as highly insulating materials with very low conductance [1].

Spectrum analyzers and Fourier analyzers can also be used for impedance measurements at audio and higher frequencies, even spectrum analyzers do not provide phase information [16]. In a frequency range between 100 kHz and 100 GHz the impedance measurement can be performed using a network analyzer [40]. Measurements of the transmission through and/or reflection from a material are used together with information about the physical dimensions of the sample to characterize the electrical properties [16].

Figure 2.10: Commercially available system: Solartron 1260 A (left) and NPS 1890 (right).

Chapter 3

Portable EIS System

This chapter begins with an insertion of the present work in the one previously developed by the team of GEI. The hardware developed to perform bioimpedance spectroscopy is described. An overview of the software, analysis processing and performance features are presented.

3.1 Context

The Electrical Impedance Spectroscopy system (i.e., hardware and software interface) was fully developed before the start of this project. Thus, the present work included the performing tests and some software modifications for further applications.

3.2 Portable Electrical Impedance Spectroscopy System

The portable EIS system conceived and constructed at GEI, called bioimp. V.4.0 mini, is able to performed linear or logarithmic AC scans from 1kHz to 5 MHz. The system implements the phase sensitive detection, PSD, method and can drive either a current or a voltage signal to excite a biological sample.

The design specifications are listed in following table.

Table 3.1: Summary of specifications of the EIS system.

	Range	
Parameter	Current Mode	Voltage Mode
Measuring method	2 electrodes	
Frequency	1 kHz to 5 MHz	
Signal amplitude	25 µA	4.6 V
Impedance magnitude[3]	100 Ω to 100 kΩ	1.5k Ω to 2.2 MΩ
Impedance phase	-π rad to π rad	-π rad to π rad
Mean absolute magnitude error	1675.45 Ω	709.37 Ω
Mean absolute phase error	2.45 ^{0}	2.06 ^{0}
Mean distortion	0.29 %	0.48 %
Mean SNR	117.0 dB	118.8 dB
Calibration	Automatically calibrated by software	

3.3 System Design

The conceived system employs two electrodes and consists of three main modules: signal conditioning unit, acquisition system (PicoScope®3205A) and a laptop for data processing (Matlab® based software), as Figure 3.1 depicts.

[3] The range of impedance magnitude, measured by the EIS system, is likely to be extended by the adjustment of the system's gain.

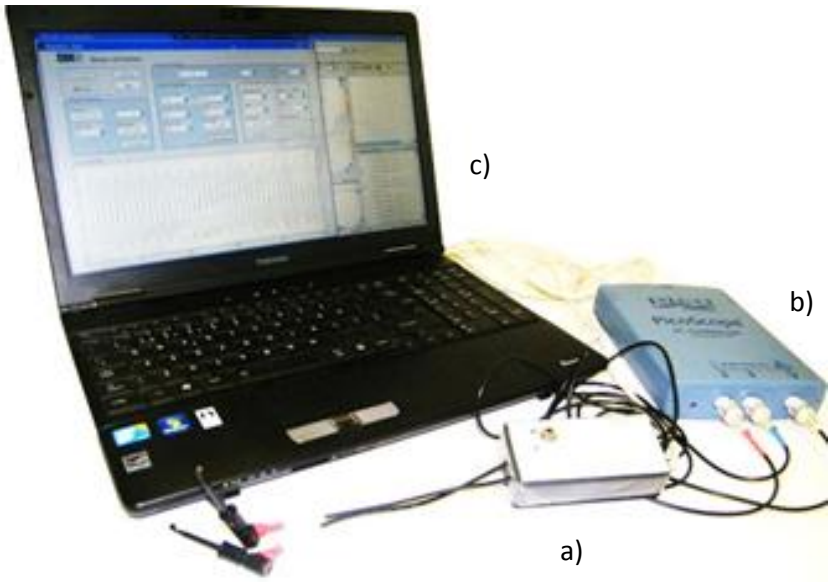

Figure 3.1: EIS System: a) bioimp. V.4.0 mini; b) PicoScope®3205A; c) Laptop with data processing algorithms.

The electrodes being used are beryllium cooper gold platted needles with around 1.02 mm in diameter and the cables that connect the sample and the conditioning unit are short as possible RG174 RF coaxial cables and are used for optimized Signal to Noise Ratio. The digital oscilloscope PicoScope®3205A has dual functionality: 1) synthesizes and provides the excitation AC signal to the conditioning unit (ADC function); 2) digitalizes both excitation and induction signals at high sampling rates (12.5 MSps) and transfers data to the computer via USB where it is stored. The signal conditioning unit receives the exciting AC signal, coming from the PicoScope®3205A, and amplifies it to be applied, through an electrode, to the specimen under study. The induced AC signal is collected by a second electrode and is redirected to the conditioning unit where it is also amplified. Both excitation and induced signals are conduced to the PicoScope®3205A to be digitalized.

The following block diagram synthesis the EIS system operation.

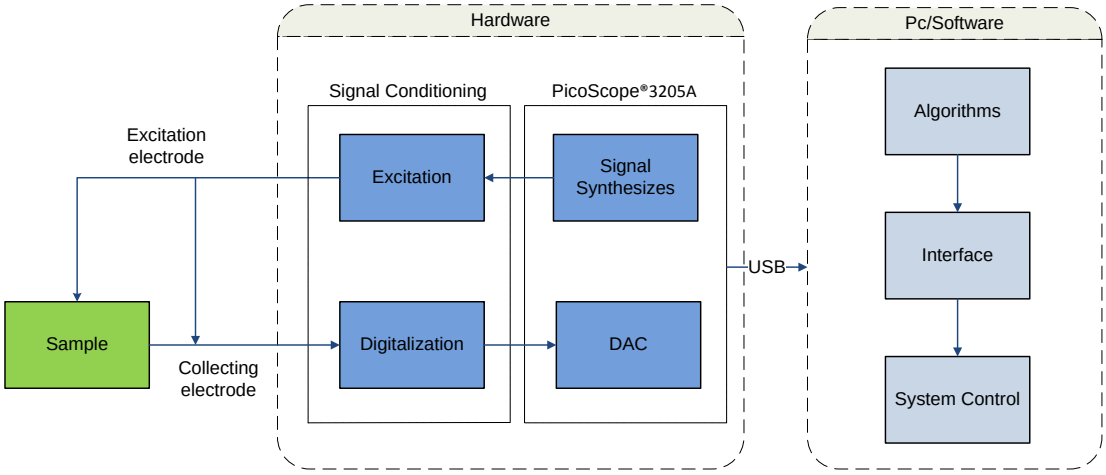

Figure 3.2: Flow chart of the EIS system.

As previously mentioned, the type of excitation depends on the type of application and the conceived system is prepared to operate in both excitation modes. The selection of the operation mode is carried out by an external switch that the conditioning unit has (see electronic circuit schematic in Appendix A). As the Figure 3.3 and Figure 3.4 depict, the two types of excitation modes have different features that can be synthesized.

The current mode circuit employs the current-feedback amplifier AD844 in a non-inverting ac-coupled CS configuration (see Figure 3.3), already studied by R Bragós *et al* 1994[41].

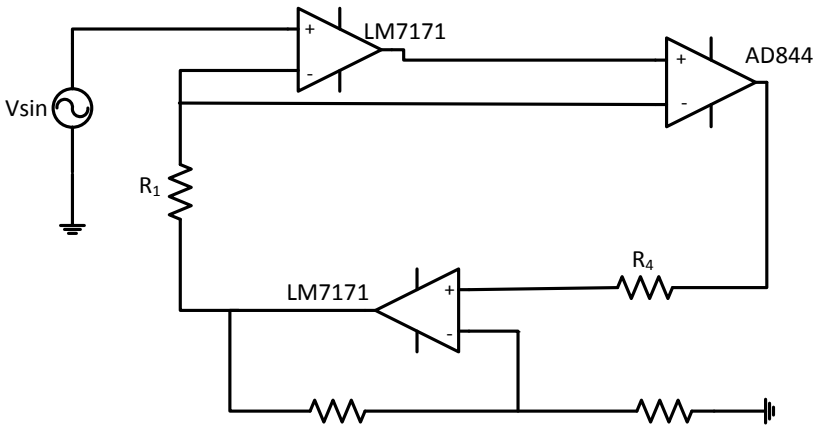

Figure 3.3: Schematic Diagram of Current Source.

In the voltage mode circuit a high speed voltage-feedback amplifier LM7171 is employed. This behaves like a current-feedback amplifier due to its high slew rate, wide unit-gain bandwidth and low current consumption [42]. Nevertheless it can be applied in all traditional voltage-feedback amplifier configurations [42], as the one used (see Figure 3.4) .

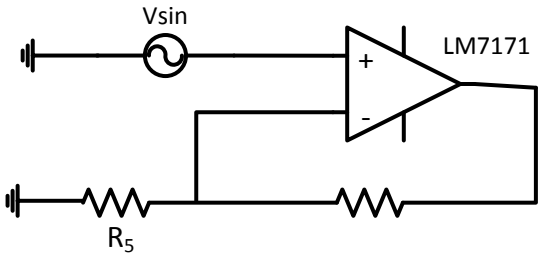

Figure 3.4: Schematic Diagram of Voltage Source.

The current or voltage signals resulting of each mode are sensed by a high speed operational amplifier, LT1220, which performs reduced input offset voltage and is able of driving large capacitive loads [43].

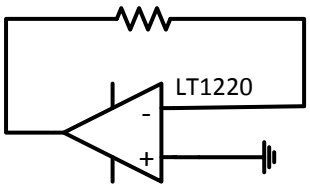

Figure 3.5: Schematic Diagram of high speed operational amplifier.

The gain values of both excitation sources can be changes in order to extend the range of impedance magnitude. The gain of current excitation source is defined by $1/R_1$ and of the voltage excitation source is $1 + R_6/R_5$. Moreover, the gain of the system is defines by the transconductance gain of the LT1220.

When assessing bioimpedance some errors appear, especially at high frequencies, which correspond to high equivalent parasitic capacitances introduced by the cables and

mainly by the amplifiers. A driven shield technique can be implemented to the coaxial cables to cancel the capacitive effect and a correction algorithm is proposed to overcome phase shift and magnitude errors. Since these errors are considered to be systematic errors, they do not directly affect the results and can be discounted.

3.4 Software and Analysis Processing

The EIS system already has a software interface, developed with Matlab® tools, for driving measurements, algorithms to fit the impedance spectrum and extract bioimpedance parameters. This application has two main objectives: provides the interface between the hardware and the acquisition modules (PicoScope®3205A) and process the acquired data. The management of the acquisition is made using a library of functions (dynamic linked library) provided by the manufacturer of the PicoScope®3205A to communicate and control all operations of the signal process and acquisition modules. The acquisition process is initiated with a test communication with the digital oscilloscope followed by the configuration of signal generation parameters. The acquired data are transferred to the PC, via a USB channel, after the PicoScope®3205A memory is totally filled.

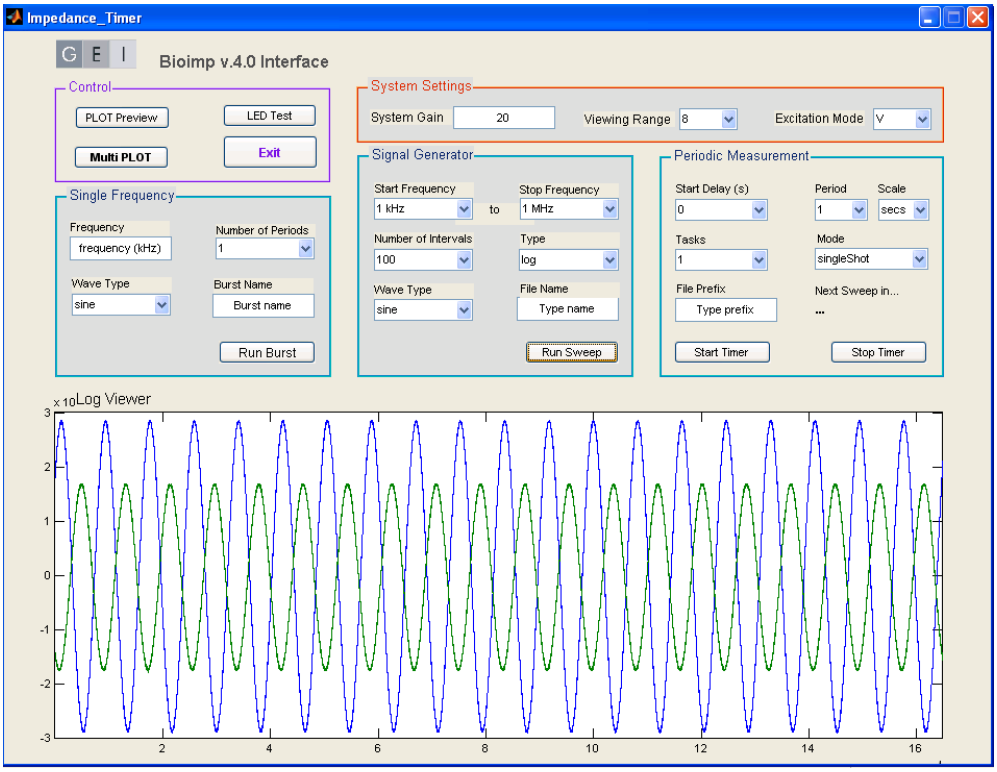

Figure 3.6: GUI to control EIS acquisition: in the blank section appear in real time the sinusoids of voltage and current.

The software allows an analysis for one specific frequency or alternatively at different frequencies for carry out a true bioimpedance spectroscopy. These two software functioning modes can be programmed for continuous monitoring, where the number of acquisitions and the intervals between them are specified by the user. The implementation of this timer ensures the collection of data for long periods, enough to allow the observation of trends in the impedance profile. The bioimpedance measurements are saved in a file (.txt or .mat) that contains information about magnitude, phase shift, real and imaginary parts of the measured impedance, for each frequency. The file is saved in a pre-determined directory with a filename, chosen by the user, with date and time associated to them. Additionally, the interface has a function that allows a graphic preview of the results, as Cole-Cole plots.

A digital Phase Sensitive Detection method, PSD, was implemented, with a novel implication, to access the impedance phase shift. In the literature this method is described as a quadrature demodulation technique that implements a coherent phase demodulation of two reference signals [44, 45]. Although, the theoretical requirements ensure that the reference signal has null phase at the origin and that its amplitude equals to 1 [44], the developed PSD method was tested without these. The algorithm was tested with Matlab® for several phases and amplitudes. For all of them the PSD method was showed a corrected phase shift assessment comparing with the results obtained with the theoretical requirements.

The following mathematical demonstration (**3.1** - **3.12**) and the schematic block diagram (Figure 3.7) supports the results and validated the developed algorithm.

The signal from the Picoscope®3205A that corresponds to the current, $V_I = Bsin(\omega t + \varphi_2)$, is set as the reference signal. Since the phase of the signal V_I is not controlled, it is easily understandable that it does not necessarily contain a null phase. This statement remains valid whether V_I is used to excite the sample, in the current mode, or whether it corresponds to the current passing through the sample, in the voltage mode. The signal from the Picoscope®3205A that corresponds to the voltage $V_V = A\,sin(\omega t + \varphi_1)$, also contains a non-null phase. Both amplitudes, A and B, are also different from each other and none equals to 1.

Assuming that the analog input signals $V_V(t)$ and $V_i(t)$ are sine waves of frequency f, amplitude A and B, respectively, and initial phase φ_1 and φ_2, respectively:

$$V_V(t) = A\,sin(2\pi ft + \varphi_1) \tag{3.1}$$

$$V_I(t) = B\,sin(2\pi ft + \varphi_2) \tag{3.2}$$

The digitized input signals $V_V(n)$ and $V_I(n)$ are obtained from $V_V(t)$ and $V_I(t)$ respectively, by sampling at a frequency, f_s , where f_s is a multiple of the f:

$$V_V(n) = A\,sin\left(\frac{2\pi fn}{f_s} + \varphi_1\right), n \in [0, N-1] \tag{3.3}$$

$$V_I(n) = B\,sin\left(\frac{2\pi fn}{f_s} + \varphi_2\right), n \in [0, N-1] \tag{3.4}$$

Where N is the number of samples. N/f_s is the measurement time and must be an exact multiple of $1/f$, so that there is whole number of cycles of the sine wave.

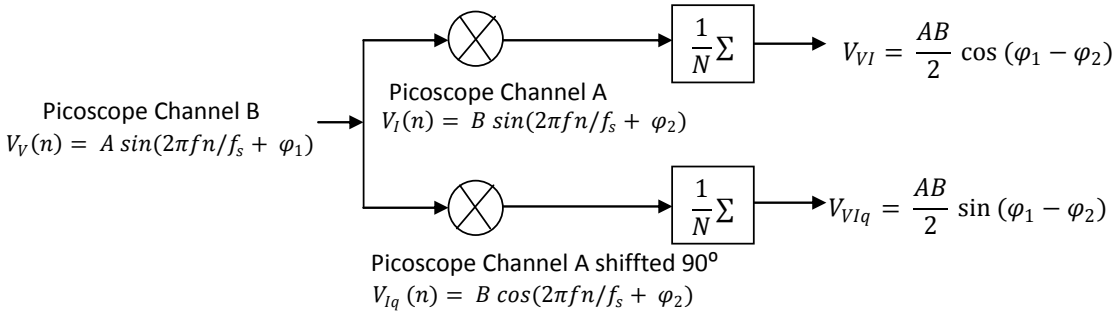

Figure 3.7: Schematic of Phase Sensitive Demodulator implemented in the EIS system

The signal $V_I(n)$ is set as reference. The quadrature reference signal, $V_{Iq}(n)$, results from the reference signal shifted by a phase of 90°. Consequently,$V_{Iq}(n)$ is cosine with the same frequency, amplitude and initial phase as $V_V(n)$.

$$V_I(n) = B\,sin\left(\frac{2\pi fn}{f_s} + \varphi_2\right), n \in [0, N-1] \tag{3.5}$$

$$V_{Iq}(n) = B\,cos\left(\frac{2\pi fn}{f_s} + \varphi_2\right), n \in [0, N-1] \tag{3.6}$$

The output voltages of the system are:

$$V_{VI} = \frac{1}{N}\sum_{n=0}^{N} V_V(n)\, V_I(n) \tag{3.7}$$

$$V_{VIq} = \frac{1}{N}\sum_{n=0}^{N} V_V(n)\, V_{Iq}(n) \tag{3.8}$$

The product between two sine signals, with the same frequency, results in a sum of a DC signal and a sine signal with a frequency that is the double of the original. The double frequency component can be suppressed since the time is a multiple of the period of the input sine signal. Therefore, it remains only the DC component which amplitude is dependent on the amplitude of the individual sine signals and their relative phase:

$$V_{VI} = \frac{AB}{2}\cos(\varphi_1 - \varphi_2) \tag{3.9}$$

$$V_{VIq} = \frac{AB}{2}\sin(\varphi_1 - \varphi_2) \tag{3.10}$$

From the expressions above, the resulting amplitude and phase can be determined:

$$\varphi_1 - \varphi_2 = arctan\left(\frac{V_{VIq}}{V_{VI}}\right) \tag{3.11}$$

$$A = \frac{2}{B}\sqrt{(V_{VI})^2 + (V_{VIq})^2} \tag{3.12}$$

The determined phase is actually a phase difference between the demodulated signal, V_V and the reference signal,V_I, i.e., it corresponds to the phase difference between voltage and current signals. Figure 3.8 shows the consistence of the algorithm when the impedance phase of a real data is compared with a spice simulation in Cadence®.

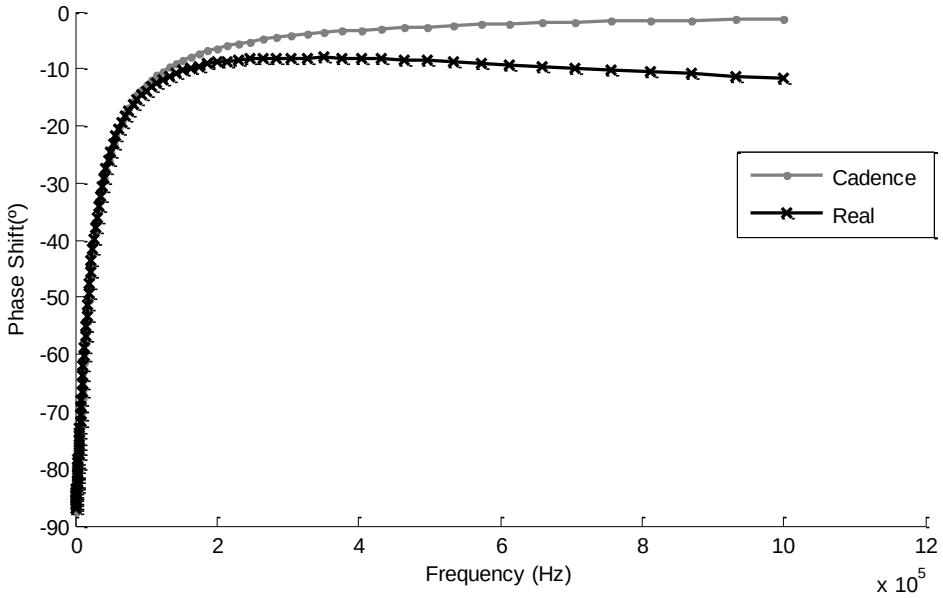

Figure 3.8: Comparison between impedance phase of a real data and Cadence® simulation data for a RC circuit.

The determination of impedance magnitude cannot be achieved by the PSD method, since the amplitude (equation **3.12**) shows a dependence on the amplitude of the reference signal, which, in this case, is not equal to 1. Hence, to assess amplitude, the EIS system algorithm processes the Root Mean Square, RMS, of both signals $V_V(t)$and $V_I(t)$ from de channel A and B, respectively, of the PicoScope®3205A. In this manner, the impedance magnitude is given by the ratio between the RMS value of the signal $V_V(t)$ and the rms value of the signal $V_I(t)$:

$$|Z| = \sqrt{\frac{\sum_{i=0}^{N} (V_V{}^2)_i}{\sum_{i=0}^{N} (V_I{}^2)_i}}\, Gain\ , \qquad \forall\, i\ \in [0, N-1] \tag{3.13}$$

Where *Gain* is the EIS system gain defined by the transconductance gain of the LT1220.

3.5 Performing Tests

The portable EIS system was subjected to several preliminary tests to assess its performance over the frequency range. The magnitude and phase errors, the Total Harmonic Distortion, THD, and Signal to Noise Ratio, SNR, were evaluated. The current and voltage sources behavior, as well as their internal resistance, were evaluated too.

The THD and SNR were evaluated under the load that simulates a hypothetical biological tissue and for the operating frequency range (1 kHz to 1 MHz). Both mathematical expressions were implemented in a Matlab® algorithm and the results were assessed for both PicoScope®3205A channels, and for both operating modes.

The THD was estimated for up to sixth harmonics using the following equation:

$$THD(\%) = \sqrt{\frac{V_2^2 + V_3^2 + \cdots + V_n^2}{V_1^2}}.100 \tag{3.14}$$

Where $V_1$is the amplitude of the first harmonic and $V_2, V_3, V_n$are the amplitudes of the second, third and n-th harmonics. Additionally, the THD was evaluated with the PC oscilloscope that PicoScope®3205A software provides, just to confirm the obtained values. The mean THD obtained for channels A and B, using the current operating mode, was respectively 0.28 % and 0.30 %. When using the voltage operating mode, the THD obtained was 0.35 % and 0.62 %, respectively for channels A and B.

The SNR was estimated using the following mathematical expression and the mean SNR obtained for channels A and B, using the current operating mode, was respectively 118.3 dB and 115.7dB. When using the voltage operating mode, the SNR obtained was 119.0 dB and 118.6 dB, respectively for channels A and B.

$$SNR = 20log_{10}\frac{V_{signal}}{V_{noise}} \tag{3.15}$$

Where V_{signal} and V_{noise} are the amplitudes of signal and noise respectively.

To evaluate the magnitude and phase performance of the EIS system and the current and voltage sources behavior, over the frequency range from 1 kHz to 1 MHz, were analyzed nine resistors with values between 10 kΩ and 100 kΩ.

Both magnitude and phase error remains small and almost insignificant and both increase exponentially. It is also observed that both errors have a linear dependence with the resistor value.

Table 3.2: Mean absolute errors for both operating modes

	Current Mode	**Voltage Mode**
Mean absolute phase error	2.45°	2.06°
Mean absolute magnitude error	1675.45 Ω	709.37 Ω

To accomplish the analysis of the sources behavior it has been recorded the output signal of the LM7171 amplifier, for the voltage operation mode, and the output signal of the AD844 amplifier, for the current operation mode. The VS behaves very consistently for the different analyzed loads, however the CS behavior is much more consistent. The dependence of the source behavior with the load is more noticeable and the loss in frequency is increased for greater loads.

The internal resistance of the CS corresponds to the internal resistance of the transconductance output of the AD844. From the datasheet [46] this resistance has a typical value of 3 MΩ. In relation to the VS, the internal resistance value was not known whereby it was evaluated. To perform this task, there were saved the excitation signal of the PicoScope®3205A output and the signal of the LM7171 output, for the same nine resistors. The internal resistance value was calculated using the following expression, which was implemented in a Matlab® algorithm:

$$R_{int} = R_L * \frac{V_S - V_L}{V_L} \qquad 3.16$$

Where R_{int} is the internal resistance, R_L is the load (resistor), V_S is the signal output of the PicoScope®3205A and V_L is the output signal of the LM7171. The determined value is around 2.5 kΩ and it varies slightly with the load value. For high frequencies (from 500 kHz onwards) the internal resistance value increases exponentially with frequency (see Figure 3.9).

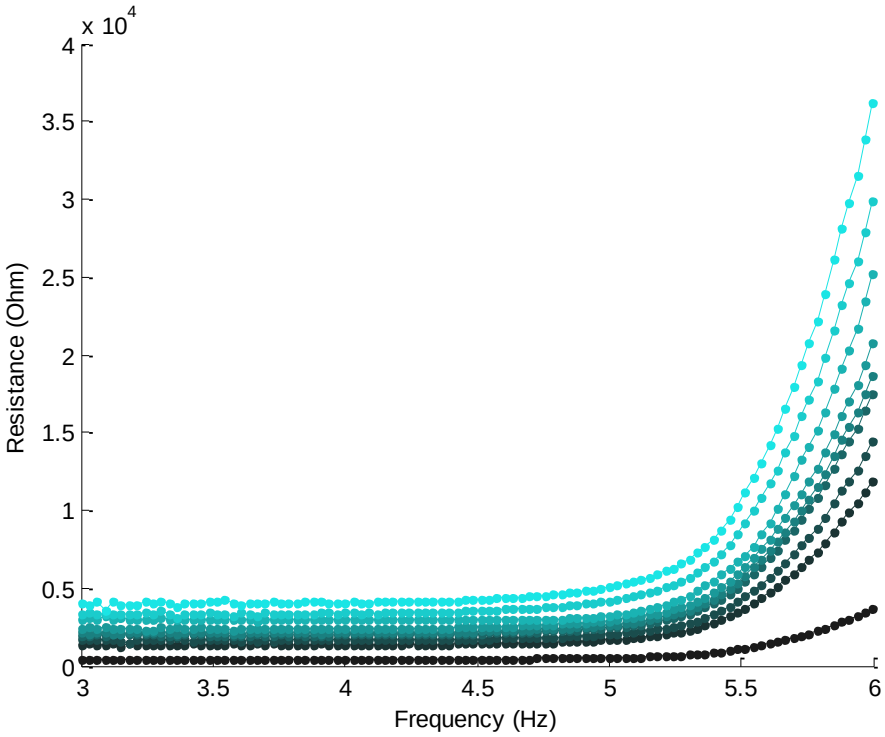

Figure 3.9: Internal resistance variation over the frequency for several resistor loads with values between 10 kΩ and 100 kΩ for the voltage source.

Chapter 4

Broadband Signals Simulation

This chapter is entirely dedicated to broadband signals simulation. The chapter begins with presentation of the signals followed by the simulation results. A brief discussion about which is the best signal and which features should have a possible hardware is sketched.

4.1 Signals

As already mentioned in the Chapter 2 different broadband signals can be used to performer bioimpedance measurements. Moreover, it was important to execute some simulations in order to prove the concept of broadband excitation in the bioimpedance spectroscopy field.

Different signal types with different features were tested, but only the most interesting will be presented herein. Table 4.1 summarizes some of the used signals and their features.

Table 4.1: Examples of simulated signals and their features.

Type		Features	Waveform
Gaussian	$f(x,\mu,\sigma) = \frac{1}{\sigma\sqrt{2\pi}} e^{-\frac{1}{2}\left(\frac{x-\mu}{\sigma}\right)^2}$	$\mu = 0{,}5\Delta t$ $\sigma = 0{,}01\Delta t$ $\Delta t = 500\mu s$	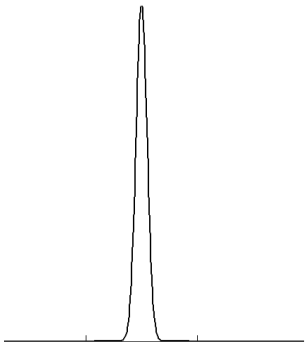
Gaussian	$f(x,\mu,\sigma) = \frac{1}{\sigma\sqrt{2\pi}} e^{-\frac{1}{2}\left(\frac{x-\mu}{\sigma}\right)^2}$	$\mu = 0{,}5\Delta t$ $\sigma = 0{,}01\Delta t$ $\Delta t = 500\mu s$	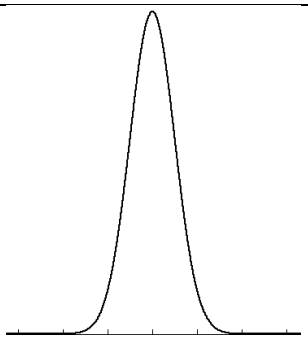
Sinc	$sinc(x) = \frac{\sin(\pi x)}{\pi x}$	$x = 800\,ns$	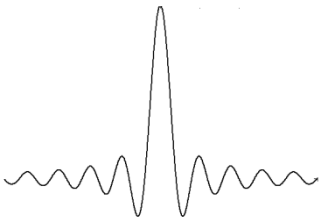
Haversinc	$haversic = \frac{sin^2(\pi x)}{\pi x}$	$x = 800\,ns$	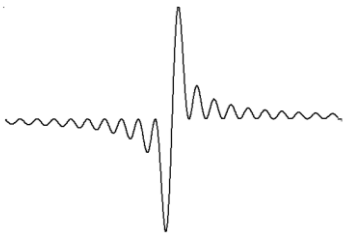

4.2 Procedures

The first step to perform further simulations was set all the signals. So, most of them were set on Matlab® and others, like rectangular pulse, were directly set in the Orcad Capture from Candence®. The simulations profiles were obtained using PSpice A/D from Candence®, after importing the signals there.

Although the main interesting was to test an equivalent circuit for biological application it was important to test a purely resistive load, once it was known the expected results.

The following figure depicts the simulation of a single resistor with the excitation by a Gaussian pulse with time duration of 50 ns and 2 V of amplitude.

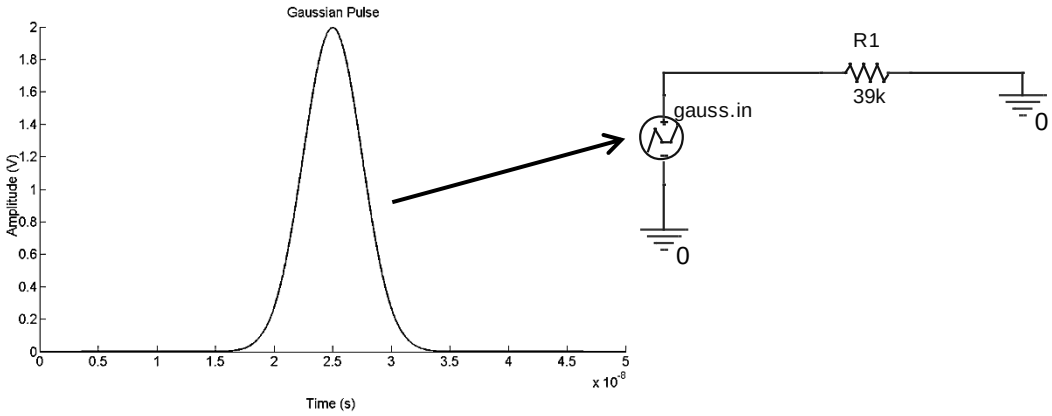

Figure 4.1: Resistive load excited by a Gaussian pulse. Gaussian pulse (left) and used circuit (right).

Two signals (voltage and current signals) were generated in Orcad and allowed the evaluation of the impedance parameters using Matlab® algorithms. In this simulation the magnitude must be equal to the resistor value and the phase shift must equals to zero, producing a single point in the Cole diagram. Besides that the results were not perfect, like a straight line at the referred values and are affected by numerical noise.

The solution was the selection of the most linear zone of the signal which implies a frequency range reduction and the achievement of the expected results.

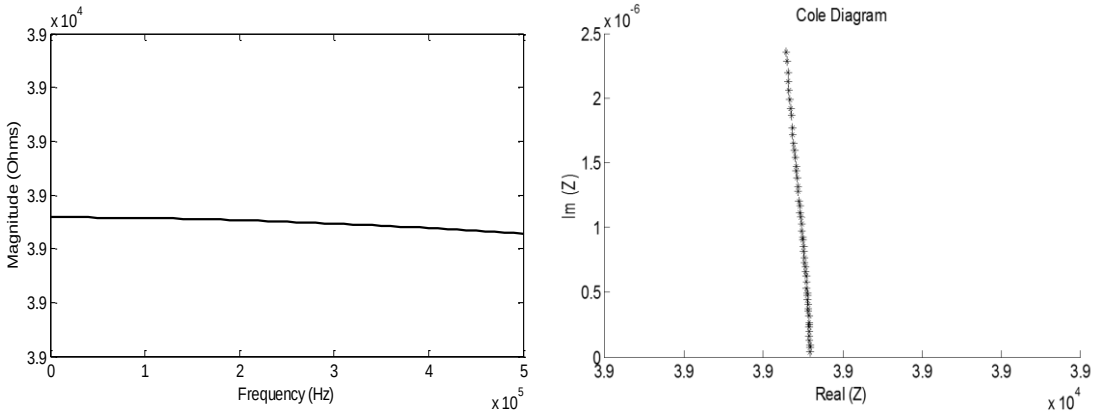

Figure 4.2: Bode (left) and Cole (right) diagrams after the noise reduction.

This simulation was held for different signals and the results were consistent with those shown above.

After the described proceeding a single cell that represents a hypothetical biological tissue could be tested. The simulations were performed using the circuit present in Figure 4.3, with different signals as the input signal.

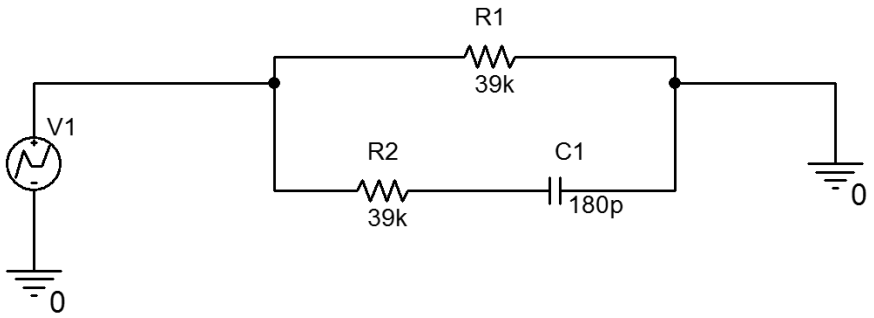

Figure 4.3: Equivalent circuit for a biological tissue.

The following results were evaluated using the same procedures described above.

4.3 Results

It is important to remark that in this section only the results from some signals will be presented since they were the ones that showed the best results.

Therefore, the Gaussian pulse was the most tested based on its features, such as its Fast Fourier Transform and the possibility of vary different parameters (μ and σ), as the Table 4.2 depicts.

Table 4.2: Gaussian pulse parameters.

	$t_{acquisiton}$	Δt	μ	σ
Gauss 1	$1\ ms$	$500\ \mu s$	$0{,}5\Delta t$	$0{,}01\Delta t$
Gauss 2	$1\ ms$	$500\ \mu s$	$0{,}5\Delta t$	$0{,}02\Delta t$
Gauss 3	$50\ \mu s$	$50\ ns$	$0{,}5\Delta t$	$0{,}05\Delta t$

The first two Gaussian pulses presented differ only in the σ parameter, which reflects the width of the pulse. So, the Gauss 1 is narrowest than Gauss 2 although all other parameters being equals.

4.3.1 Gaussian Pulse 1

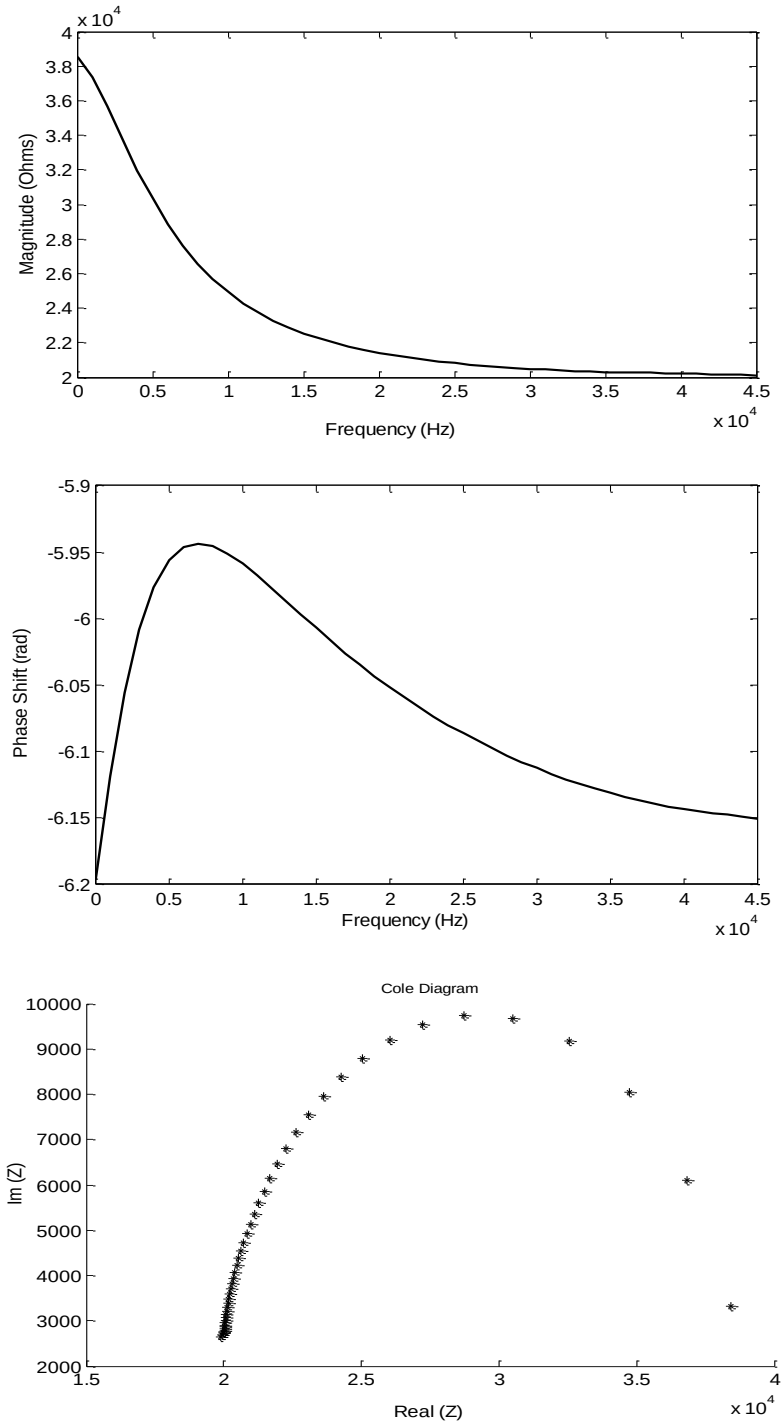

a)

b)

c)

Figure 4.4: Bode and Cole diagrams obtained by simulation of Gauss 1 for the hypothetical tissue: a) Bode magnitude plot; b) Bode phase plot and c) Cole diagram.

The Bode diagrams showed in Figure 4.4 are very consistent with the expect results. At low frequencies the current does not flow to the series arrangement connecting $R_2$to C_1. So, the current flow exclusively through R_1providing a measure of its ohmic value, as Figure 4.4 a) depicts.

However, the phase shift should increase from zero, which does not occur. Yet the Cole diagram produced shows a known distribution although most of the points are shifted to high frequencies.

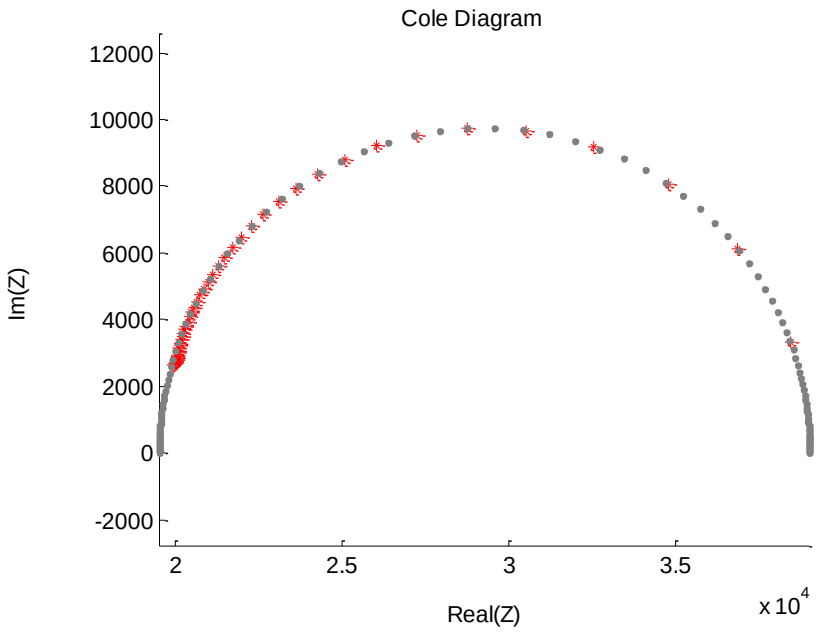

Figure 4.5: Cole-Cole fitting for the impedance data. Data from Gauss 1 excitation (red) and generated by Cole equation parameters (gray).

The Figure 4.5 depicts the Cole fitting of the data from the Gauss 1 excitation with impedance data generated by Cole equation. The theoretical Cole is accurate enough to fit the data from the simulation. This might suggest that this Gaussian pulse could be an alternative to the chirp excitation.

4.3.2 Gaussian Pulse 2

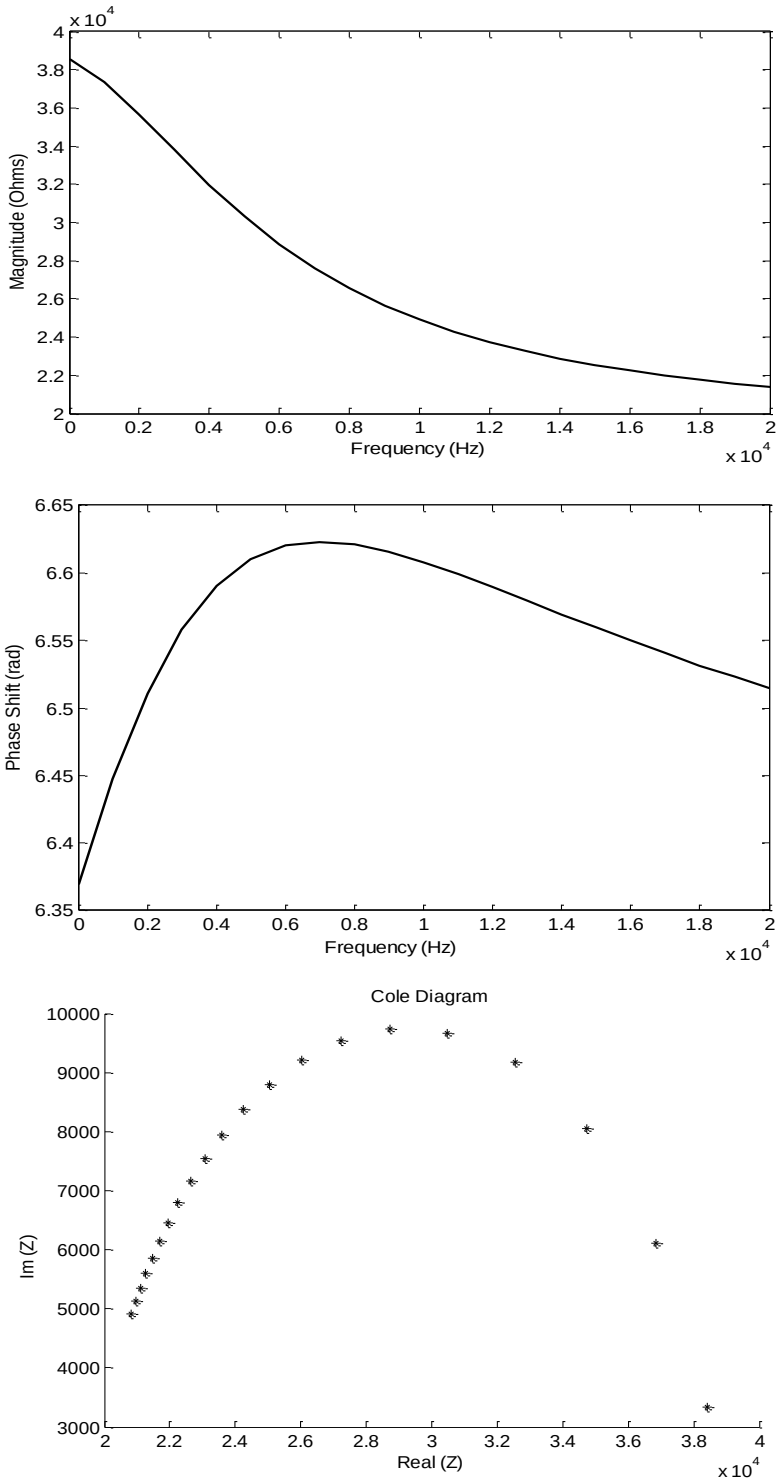

Figure 4.6: Bode and Cole diagrams obtained by simulation of Gauss 2 for the hypothetical tissue: a) Bode magnitude plot; b) Bode phase plot and c) Cole diagram.

Comparing the Bode plots of Figure 4.6 with ones of obtained with Gauss 1 some noticeable differences appear. The most relevant is the phase shift and the decreasing of frequency range. Yet the Bode magnitude plot presents the expected values and the Cole diagram shows a similar distribution. Moreover, the Cole Diagram has fewer points in the interesting frequency range.

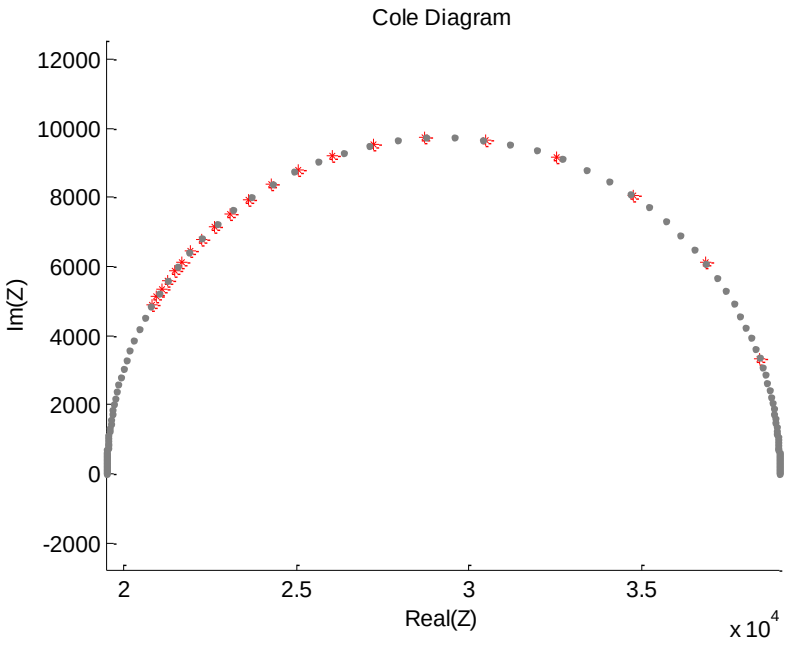

Figure 4.7: Cole-Cole fitting for the impedance data. Data from Gauss 2 excitation (red) and generated by Cole equation parameters (gray).

The data generated by Cole equation parameters fit the simulation data with good accuracy. However, the reduced number of points produces a heterogeneous distribution along the theoretical Cole, since most of them are shifted to high frequencies.

4.3.3 Gaussian Pulse 3

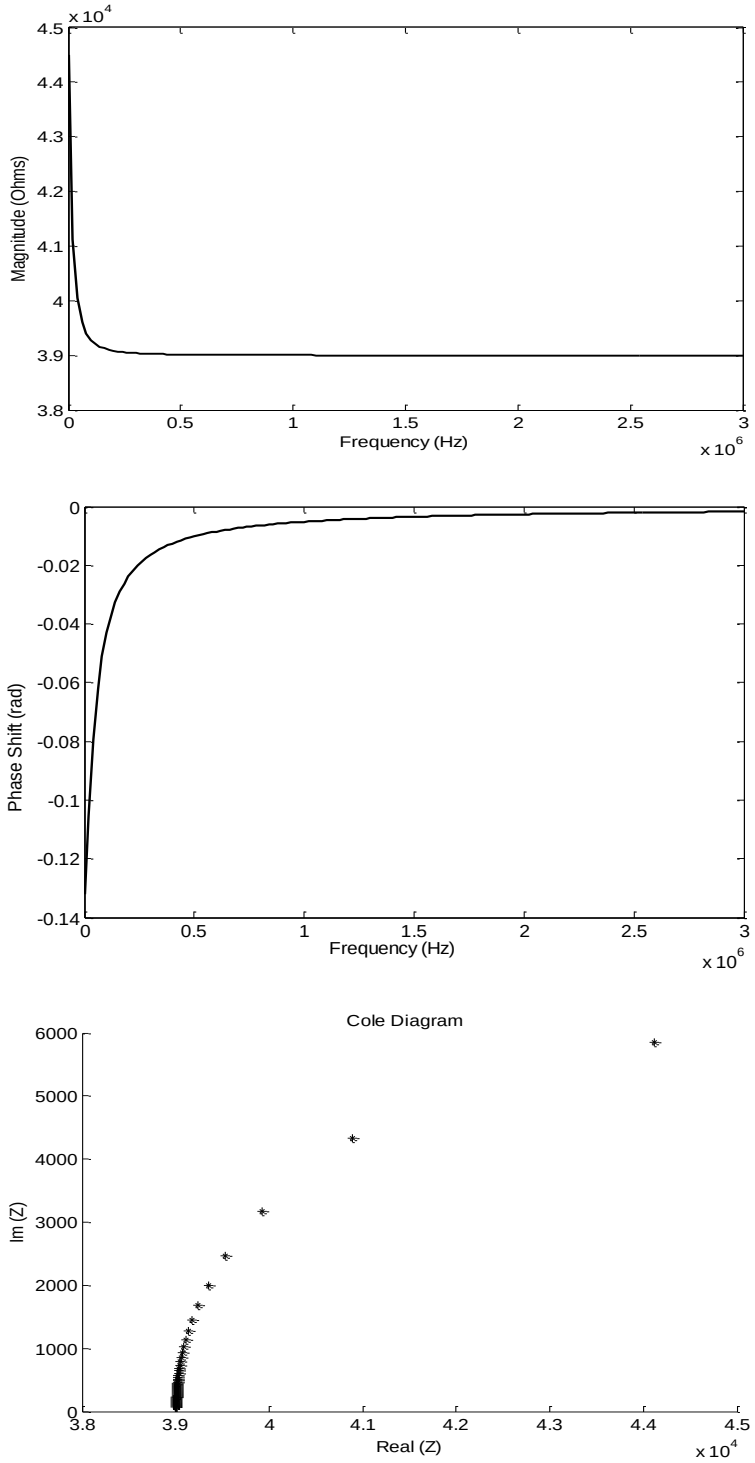

Figure 4.8: Bode and Cole diagrams obtained by simulation of Gauss 3 for the hypothetical tissue: a) Bode magnitude plot; b) Bode phase plot and c) Cole diagram.

The Bode diagrams shown in Figure 4.8 have a graphical behavior expected. But the magnitude and phase shift values are unexplained comparing to the theoretical ones. The Bode magnitude plot should decreases from the ohmic value of R_1 to values near 20 kHz at higher frequencies.

This Gaussian pulse has a low pulse duration which reflects the increase of the frequency range. However, most of the Cole points are displaced to the value corresponding to low frequencies.

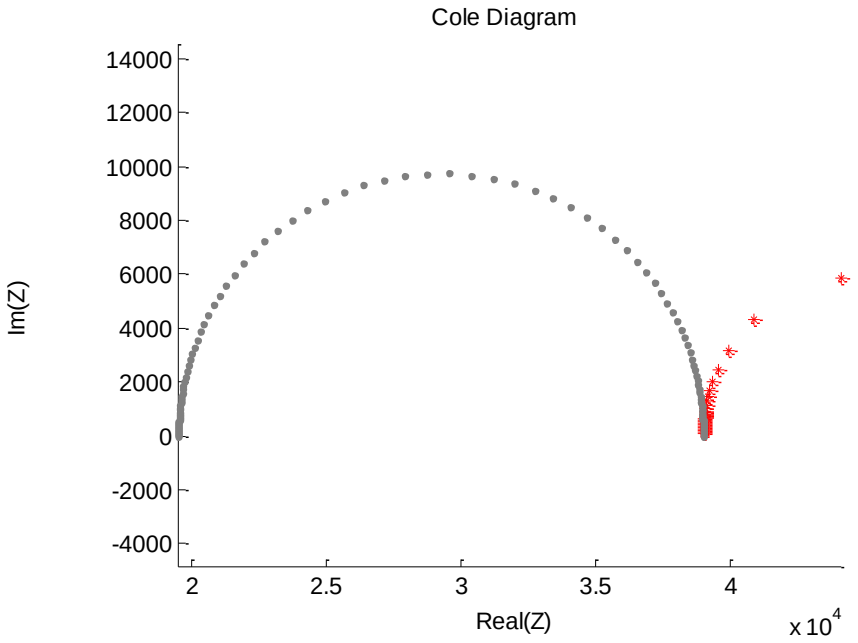

Figure 4.9: Cole-Cole fitting for the impedance data. Data from Gauss 3 excitation (red) and generated by Cole equation parameters (gray).

The Cole diagram generated by Cole equation parameters was not accurate enough to fit the impedance data from Gauss 3 (see Figure 4.9). However the two Cole diagrams are coincident at low frequencies. This may suggest that this pulse is not a good choice for the common biological application. It is not able to perform impedance measurements in the hypothetical tissue considered.

Besides the Gaussian pulses also the Sinc and Haversinc pulses were tested and evaluated its results based on the same procedure.

Table 4.3: Sinc and Haversinc pulses parameters

	$t_{acquisiton}$	Δt
Sinc	$100\ \mu s$	$800\ ns$
Haversinc	$100\ \mu s$	$800\ ns$

As depicted in the Table 4.3 the two following signals only differ in the waveform since the acquisition features are the same. Once again the procedures and data algorithms processing were the same as the implemented in Gaussian pulses.

4.3.4 Sinc Pulse

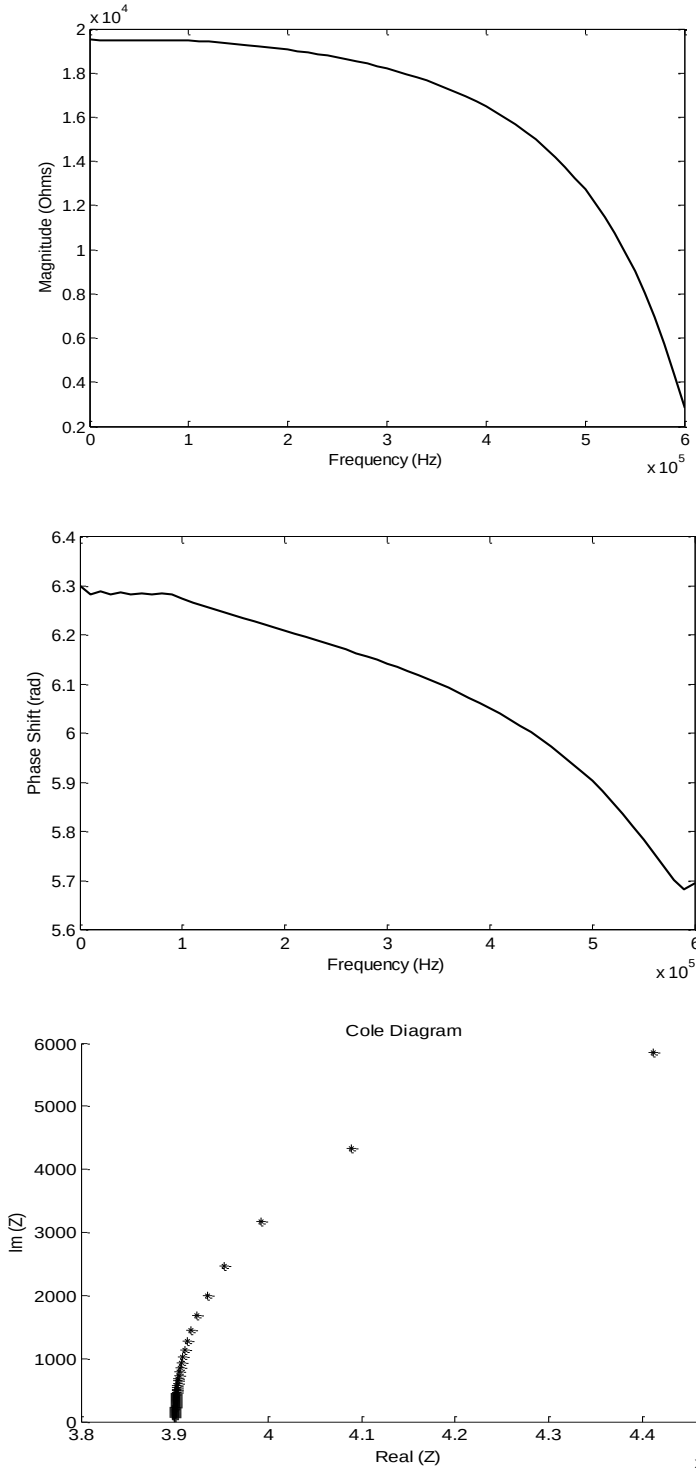

Figure 4.10: Bode and Cole diagrams obtained by simulation of Sinc pulse for the hypothetical tissue: a) Bode magnitude plot; b) Bode phase plot and c) Cole diagram.

The Figure 4.10 depicts Bode diagrams with unexplained values comparing to the expected ones. The magnitude decreases to values near zero and the phase shift also decreases in spite of increasing from zero. Even then, the Cole diagram has a known distribution with lower imaginary and real values.

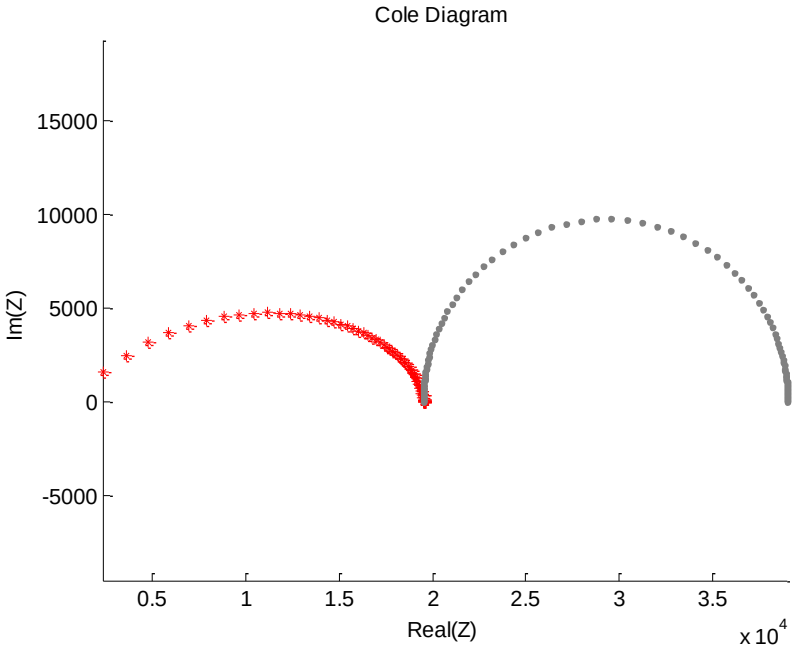

Figure 4.11: Cole-Cole fitting for the impedance data. Data from Sinc pulse excitation (red) and generated by Cole equation parameters (gray).

The Cole fitting with the Cole equation parameters has coincident values at high frequencies.

This observation may allow concluding that this signal could be used for impedance measurements at highest frequencies.

4.3.5 Haversinc Pulse

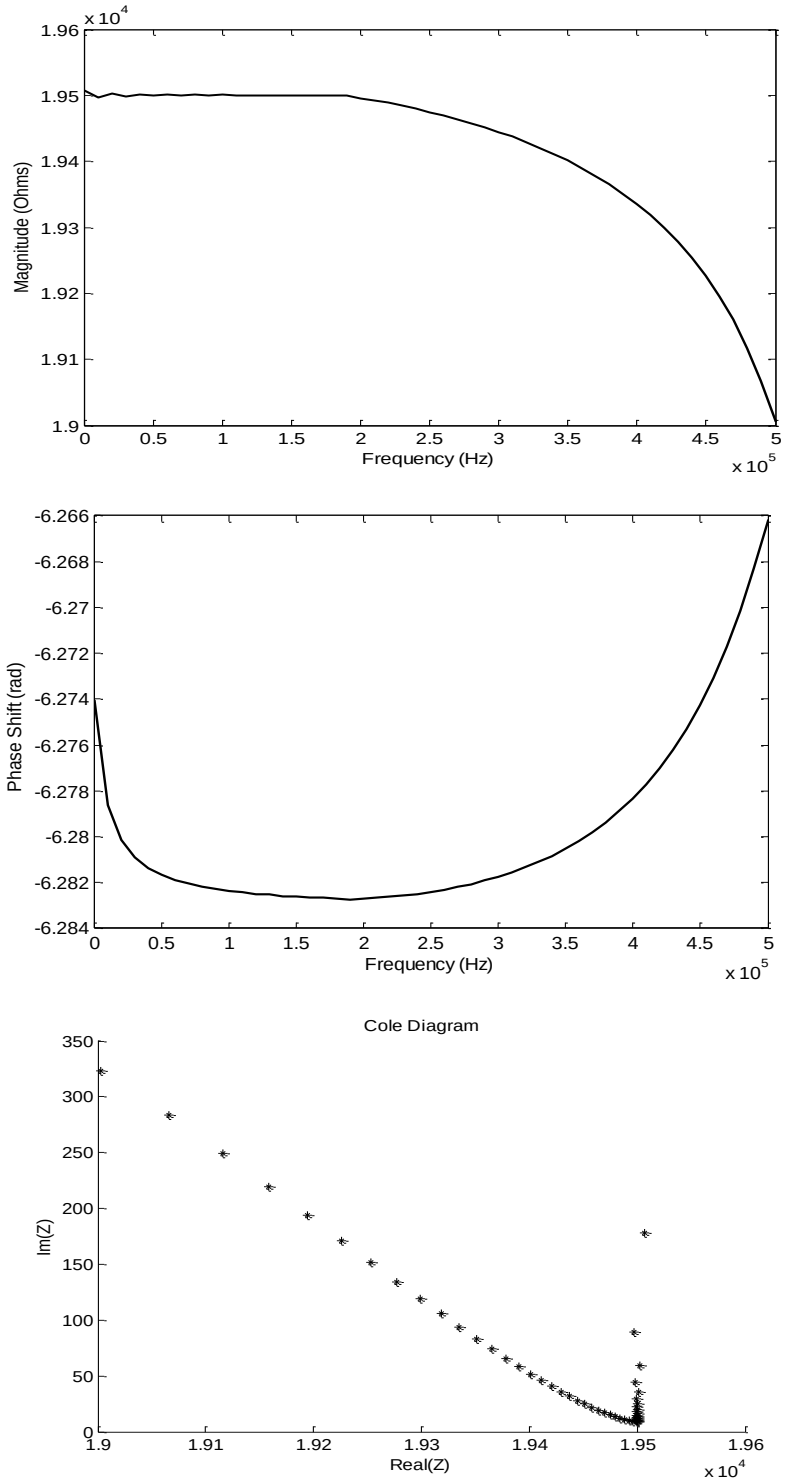

Figure 4.12: Bode and Cole diagrams obtained by simulation of Haversinc pulse for the hypothetical tissue: a) Bode magnitude plot; b) Bode phase plot and c) Cole diagram.

The Cole diagram obtained with Haversinc 1 simulation has lower impedance values resulting from the slight variation of the magnitude and the phase shift. The results are very different than the already shown.

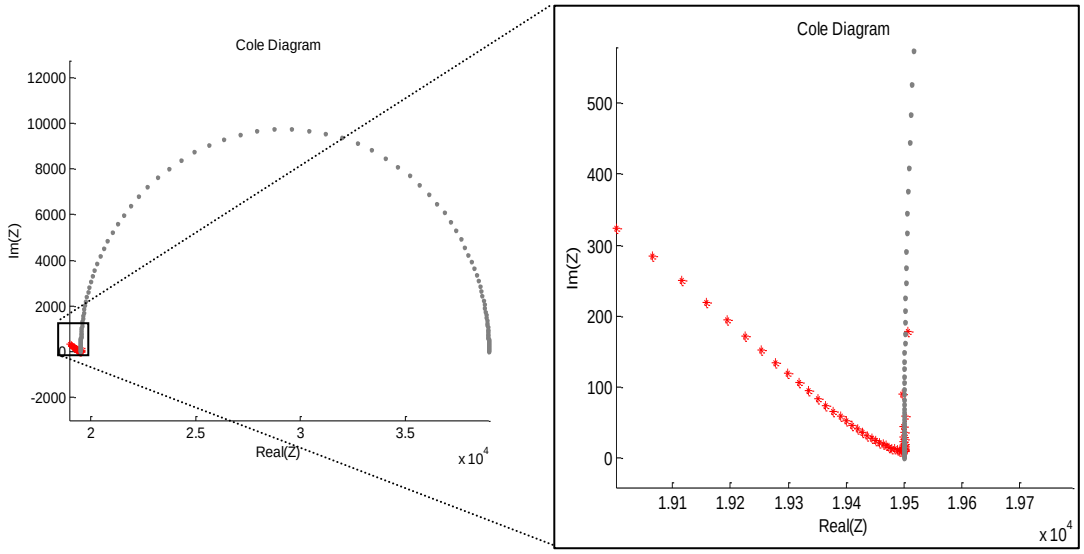

Figure 4.13: Cole-Cole fitting for the impedance data. Data from Haversinc pulse excitation (red) and generated by Cole equation parameters (gray).The right side depicts the zoom in on the marked area.

As the expected the data simulation fit is very difficult. The zoom in on the indicated area in the Figure 4.13 depicts a coincident zone at high frequencies. But the slight variation of the real and the imaginary components precludes a better conclusion.

4.3.6 Chirp Pulse

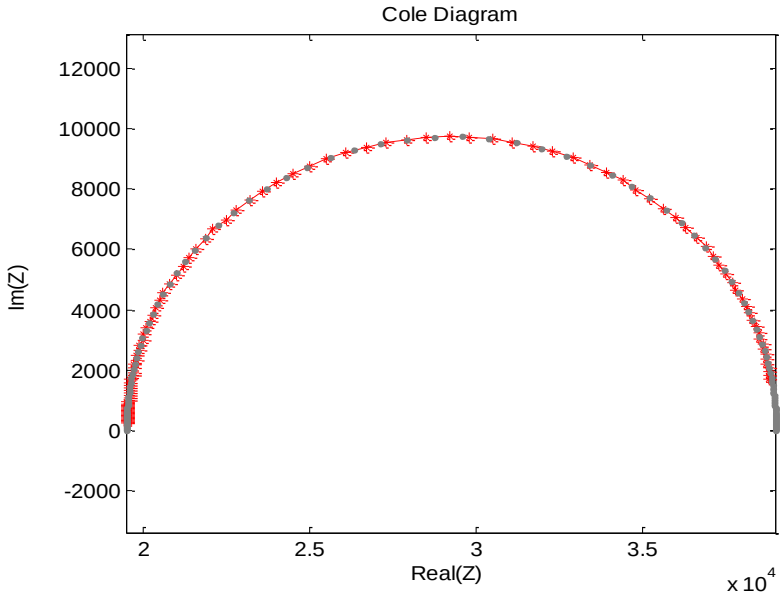

Figure 4.14: Cole-Cole fitting for the impedance data. Data from chirp excitation (red) and generated by Cole equation parameters (gray).

The Cole fitting for the impedance data from chirp excitation is depicts in Figure 4.14. The excitation of a hypothetical tissue with the chirp signal produces a Cole diagram very similar to the produced by the Cole equation parameters. In spite of the accurate fit of the simulated data is possible to identify an increase of points at high frequencies.

4.4 Discussion

The presented results must be compared with the Cole diagram resulting for the chirp excitation. As the main objective of this Chapter, it can be concluded that a signal with Gauss 1 characteristics is an alternative choice for the chirp excitation.

The variability of magnitude and phase shift values can be justified based on the numerical noise presented in all of the simulation. Thereby, the selection of a linear zone of the signal may introduce some inconsistencies. Additionally, the Fourier Transform spectrum of the most signals has few points within desire range of the spectrum.

Despite the inconsistencies, all data resulting from broadband simulation has coincident points with the theoretical Cole diagram. These results can be justified by the need of several points and high sampling rate, although the signals have been generated with a reasonable number of points for the algorithms performance. Additionally, the main conclusion resulting for the simulation is that there are signals preferable to study low frequencies and others for high frequencies. These signals may be important for the improvement of previous studies in which it becomes difficult to access low (below 50 kHz) and high frequencies due to interferences α and γ, respectively.

In order to the discussed above, a possible hardware must be able to produces well defined pulses with high sampling rates. Since the main advantages will be the adaptability of frequency range using different broadband signals.

Chapter 5

Hardware – Experimental Setups

This chapter deals with two experimental setups for bioimpedance measurements using broadband excitation signals. Both systems were conceived in order to prove the applicability of the simulated signals, actually. The results are showed and discussed.

5.1 Experimental Setup 1

The first setup uses the bioimp V.4.0 mini, already presented, the Picoscope®3205 A and an Agilent©33220 A as the signal generator. All that acquisitions parameters were controlled and defined in the software interface, developed with Matlab® tools.

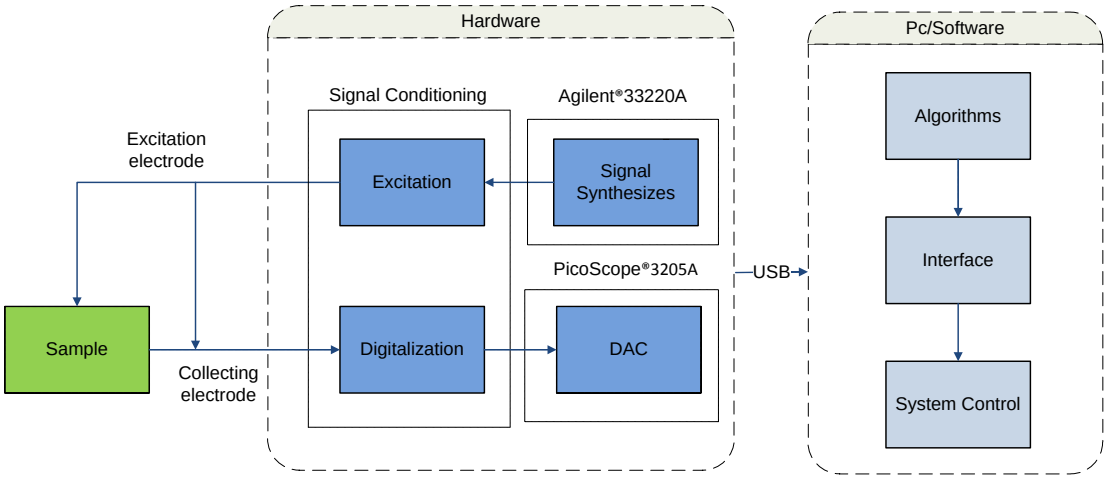

Figure 5.1: Flow chart of the Experimental Setup 1.

5.1.1 Data Acquisition

The acquisition was performed using a hypothetical cell as depicts in Chapter 4. A Gaussian pulse with the characteristics of the Gaussian pulse 1 and 2 was used to evaluate impedance measurement in the biological field of interest.

The two signals were performed using different sampling rates and time of acquisition. Once again the results were compared to the theoretical.

5.1.2 Software Interface

The software interface depicts in Figure 5.2 developed with Matlab® tools has two main objectives: provides the interface between the hardware and process the acquired data. As the software interface of the EIS system, the acquisition process starts with a test communication with PicoScope®3205A followed by the configuration of the acquisition process. The acquired data is transferred to the PC via a USB channel. This software interface allows the operator to choose the sampling rate and the viewing range of the acquisition and has a function that allows a graphic preview of the processed results. The continuous monitoring function is not programmed because due to uncertainty about its relevance.

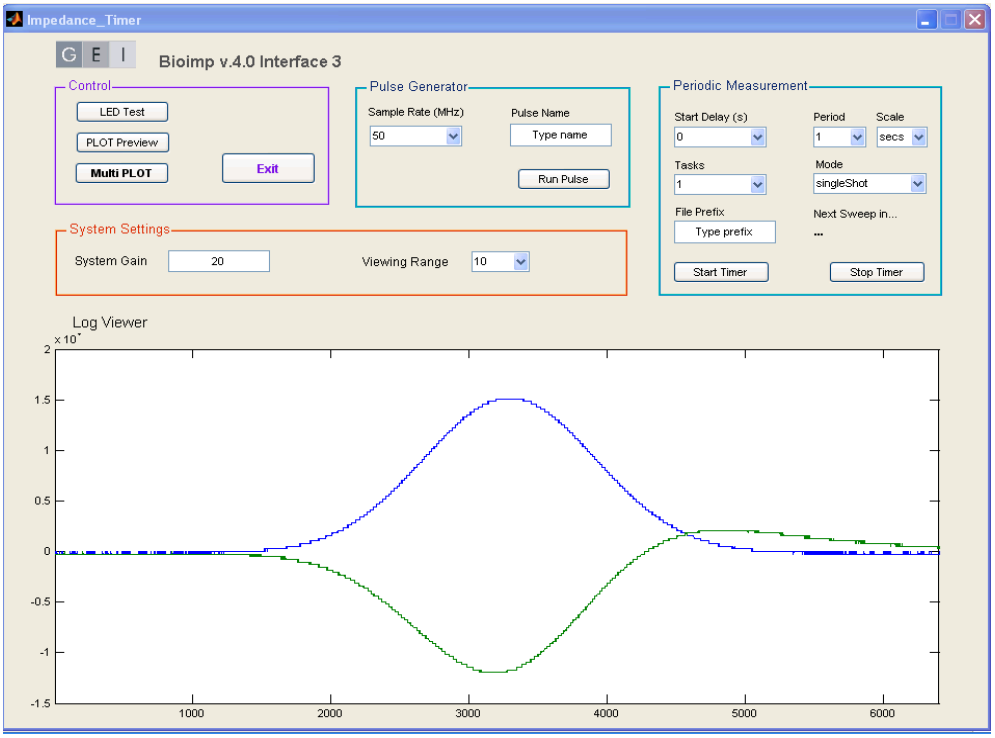

Figure 5.2: GUI to control broadband excitation acquisition.

5.1.3 Results

The Figure 5.3 shows both Cole diagrams obtained with the experimental setup for the two Gaussian pulses, already mentioned. The data was achieved during 500 µs and 20 MHz of sampling rate. The results are very consistent with simulation and the data fitting is good enough considering the used methodology. As discussed in Chapter 4 the Gaussian pulse 1 shows better results since it covers a high frequency range.

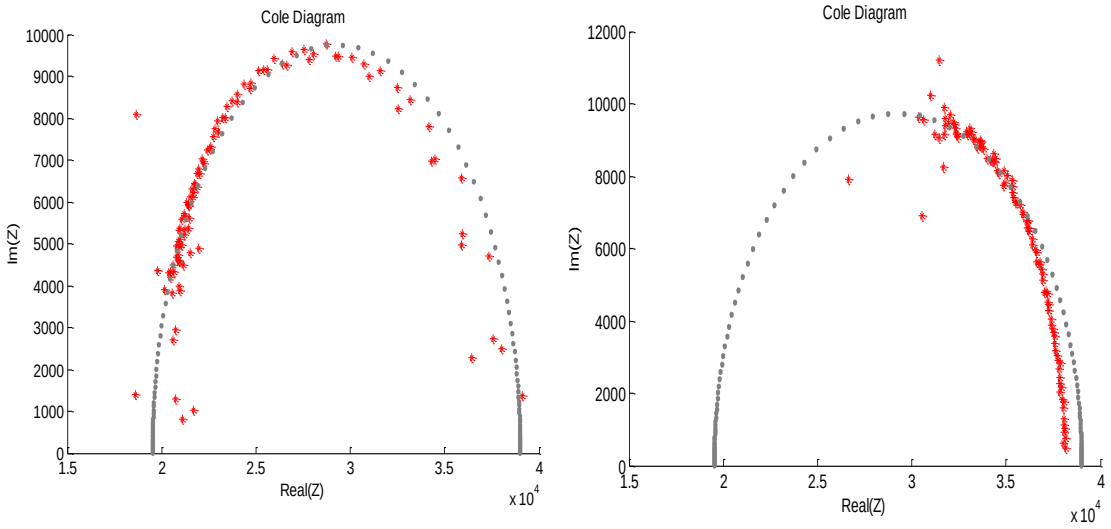

Figure 5.3: Cole-Cole fitting for the impedance data of Gaussian pulse 1 (left) and Gaussian pulse 2 (right) excitation– real data (red) and data generated by Cole equation parameters (grey).

Testing different sampling rates the obtained results for the Gaussian pulse 1 were not very distinct, since the frequency range achieved is not changed. However changing the acquisition time produces different results (see Figure 5.4).

Table 5.1: Features of Gaussian Pulse 1.

	$t_{acquisiton}$	Sampling Rate
Gaussian Pulse 1	$500\mu s$	$20\ MHz$
	$1ms$	$20\ MHz$
	$2ms$	$20\ MHz$

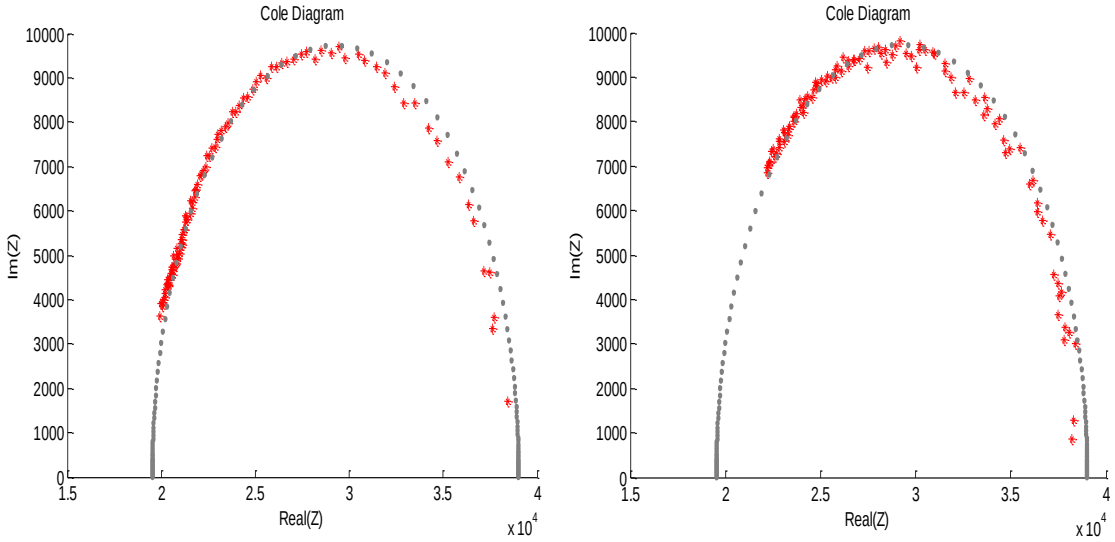

Figure 5.4: Cole-Cole fitting for the impedance data of Gaussian pulse 1 with different time of acquisition: $t_{acq} = 500\mu s$ (left) and $t_{acq} = 2ms$ (right) – real data (red) and data generated by Cole equation parameters (grey).

5.1.4 Discussion

Although only two different signals were tested using the proposed hardware, the results are quite satisfactory. Once again the Gaussian pulse 1 seems to be a good choice for the biological application field of interest. Additionally, a new observation could be drawn. The same signal can performer impedance measurements over a different frequency range changing the acquisition time.

5.2 Experimental Setup 2

Although Gaussian pulse has a very interesting frequency spectrum its physics/electronics achievement is not so simple. The solution is based on a rectangular pulse that with some filtering techniques could be approach to a Gaussian one. Thus the achievement problems can be solved and the advantage of the frequency spectrum remains.

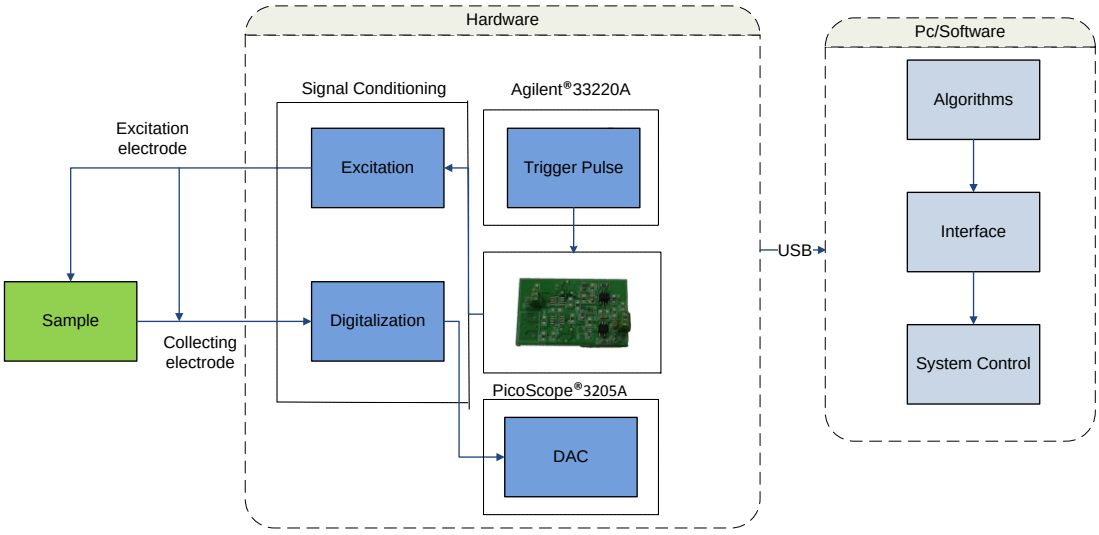

Figure 5.5: Flow chart of the Experimental Setup 2.

The experimental setup described by the flow chart in Figure 5.5 has the main modulo centered in an electrical circuit developed for generated two rectangular pulses with different width. The advantage of two consecutive pulses allows an increase of the frequency range of interest. One of the pulses is responsible for covering low frequency ranges and the other extended the frequency to higher values. Both are triggered by a pulse from the Agilent®33220A. The pulses were generated by the common timer LM555 in the time delay mode of operation. The designed electronic circuit is presented in the appendix A.

5.2.1 Discussion

The experimental setup presented in this section has the main objective to test two sequential broadband signals to cover a wider frequency range, as the literature suggests. Although many pulses width were tested any acceptable result were achieved.

Chapter 6

Biological Application Tests

This chapter besides proving the performance of the system, bioimp. V.4.0 mini, has the main purpose to verify some relation between bioimpedance and physiological parameters and infer some relation with environmental conditions and soils composition. A simple comparative test using the two type of excitation in a biological sample is presents.

6.1 Application 1

6.1.1 Motivation

The impedance parameters are correlated with physiological conditions, such as sugar level, acidity or the water content. This late is preferable used as a parameter to assess the physiological conditions of vegetables, since the water content is one the internal characteristics more important in the assessment of physiological states and it is related with the others. So, impedance parameters, such as magnitude and phase shift spectra or Z_{1k}/Z_{50k} ratio, are used as water content indicators to address the vegetables condition.

6.1.2 Data Acquisition

For impedance modelling and to draw conclusions about the variation of the impedance profile during the dehydration process seven healthy white-skinned without sprouts potatoes of the same specie with similar weight were chosen for this study.

The weight of each potato was record with a digital scale (SOEHNLE) with 0.05g precision. All potatoes were stripped for easy drying and punctured with two electrodes in apical region, which were never removed. Alternating current of 1 kHz to 1 MHz at 25 µA was passed through the biological material for impedance measurement. The acquisitions were performed every four hours and were record temperature, humidity and weight at same time. Moreover, the temperature and humidity were kept constant during all acquisitions. The temperature remained close to 25.5 °C and the humidity around 25.7 %. These parameters were measured using a digital multimeter (KAISE).

For homogeneous drying the potato position was changed at every acquisition and all the experiments were performed inside a Faraday cage to isolate the potatoes from electrical noise from lightening.

6.1.3 Results and Discussion

Generally, the analysis of bioimpedance data showed that the magnitude has increased throughout the dehydration process, especially at high frequencies while the phase shift has decreased (see Figure 6.1). Another general analysis showed that the occurrence of the maximum phase shift is verified at successively higher frequencies as the potato was getting dehydrated. This means that the capacitance inherent to the cellular membranes slightly decreased with the water loss. In fact, it was verified a mean reduction of 0.4 pF for the seven potatoes. In the other hand, the resistance associated to the extracellular fluid increased significantly (it was verified a mean increase around 50 kΩ for the seven potatoes), and the resistance associated to the cytosol also increased (it was verified a mean increase around 5 kΩ for the seven potatoes). The referred changes occurred in the potatoes' tissue in terms of Cole bioimpedance model were shown in Figure 6.2.

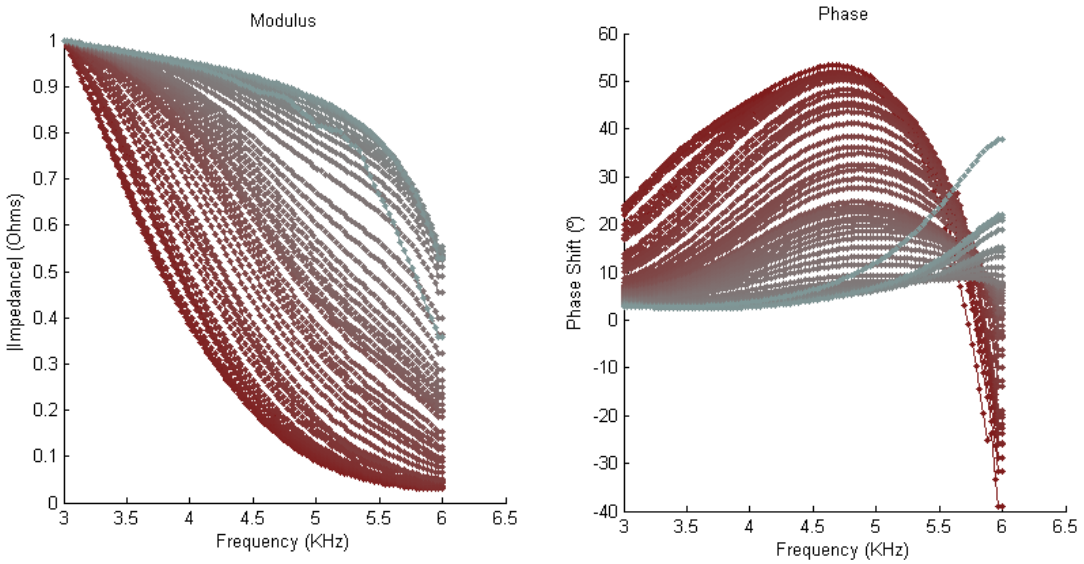

Figure 6.1: Variation of impedance magnitude (left) and phase shift (right) during the dehydration process. The gradation of colors from brown to gray is in the order: first acquired data to late acquired data (correspond to the most dehydrated state).

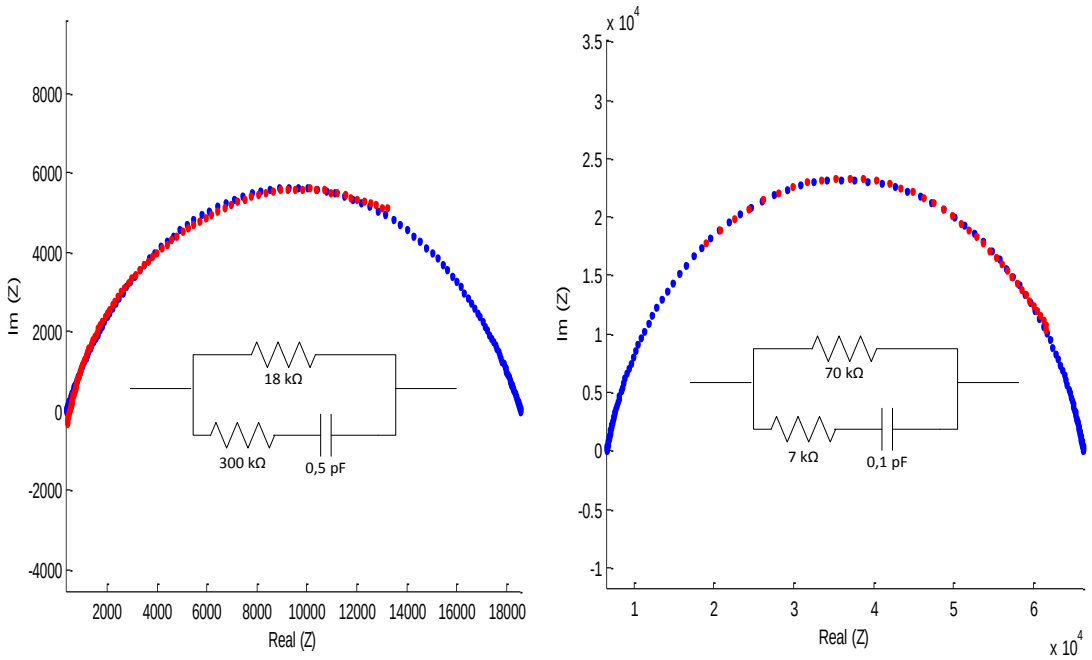

Figure 6.2: Cole-Cole fitting for the impedance data of hydrated (left) and a dehydrated (right) potato – real data (red) and data generated by Cole equation parameters (blue). The equivalent circuit for the both cases could be estimated.

The water content, WC, of potatoes was calculated by the following equation:

$$u = \frac{m_{wet} - m_{dry}}{m_{wet}}$$

Where m_{drt} is the mass of the dehydrated potato and m_{wet} is the mass of potato during the measurements along the dehydration process.

To better understand the variation of the bioimpedance profile during the dehydration process and relate bioimpedance with the WC, the ratio R_1/R_{50} was also assessed. Here, R_1 corresponds to 1 kHz, the lowest frequency the system can analyze. When expressing this index as a function of the WC, a fairly linear relationship between both is confirmed (the mean obtained for the determination coefficients,R_2, of the seven potatoes trend lines was 0.84). Thus, it is possible to assert that the ratio R_1/R_{50} gives a very approximate value of the WC of the potato, as Figure 6.3 depicts.

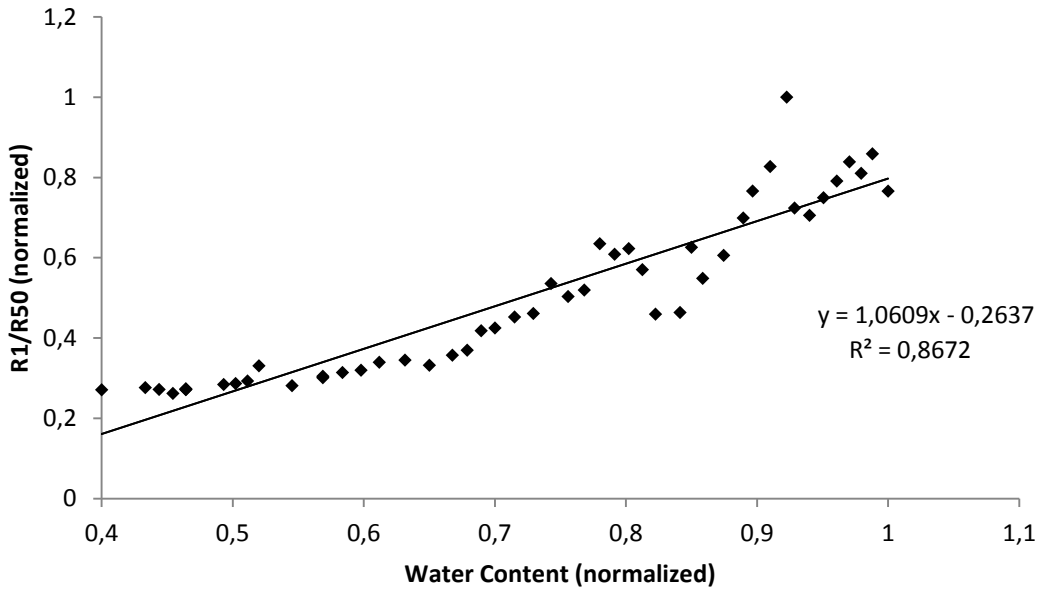

Figure 6.3: Relationship between water content and the impedance parameter R_{1k} / R_{50k}.

6.2 Application 2

6.2.1 Context

Some plant species which can be processed to provide a diesel fuel substitute have captured the interest of scientists. In this plant category, *Jatropha curcas L.* has won over the interest because of it is properties: grow on poor degraded soils and able to ensure a reasonable production of seeds with very little inputs [47]. This wild oilseed plant occurs mainly at lower altitude, so it is adapted to higher temperatures and its cultivation is predominant in Central and South America, South-East Asia, India and Africa [48].

Although the seeds of these plants are toxic to humans and to many animals, they constituted an important contribution to the economy of many countries, without competing with food production [47]. Seeds were, mostly, exported for oils extraction and soap production. Due to its drought resistant the production is provided even in marginal semi-arid lands and the fuels can be used partly to substitute costly oil imports [49].

Additionally, economic analyses have demonstrated that Jatropha can compete with Diesel and Jatropha seed oil in engines is, already, reported in the literature.

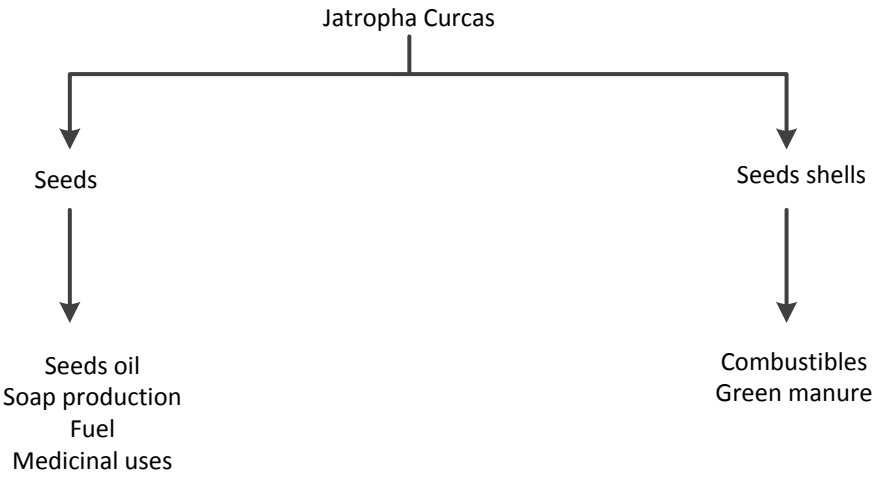

Figure 6.4: *Jatropha curcas* seeds application. Adapted from [48].

6.2.2 Motivation

Concerning the Jatropha products applications the segregation between different lines of the same plant or the segregation between cultivars of same plant product specie is really important. Based on each line or cultivar has its own impedance profile signature, it is possible to discriminate them according to its impedance profile.

A concrete application in this biology field consists in segregating seeds according to their cultivars, harvest period or origin country.

In this field the impedance data analysis uses both spectra (magnitude and phase shift) information over a convenient frequency range and also impedance parameters analysis, such as an appropriated impedance ratio.

6.2.3 Data Acquisition

Different seed cultivars from different countries and harvest season were used for this study. All seeds were cracked, the shells were carefully removed and the kernels were punctured with two electrodes in apical region. Alternating current of 30 kHz to 700 kHz was passed through the biological material for impedance measurement. The load gain of the bioimp V.4.0 mini system was changed to 1 kHz. Results from each seed were used for impedance modeling and to draw conclusions about the relationship between impedance profiles from the same cultivar, harvest in different period or in different countries.

Figure 6.5: Jatropha seeds (left) and EIS system with Jatropha seed without shell (right).

6.2.4 Results and Discussion

The Figure 6.6 shows a graphical dispersion of an impedance parameter for several seeds lines. Here, the ratio Z_{30k} / Z_{180k} corresponds to the ratio between the lowest analyzed frequency (30 kHz) and 180 kHz since it is ate this frequency that the current starts passing through the membrane.

Each plot area corresponds to a different seed line. The seeds from set 1 present higher ratio deviation in relation to the other sets. Also the seeds from the same set present a higher impedance variation. This suggests that seeds from set 1 have distinct electric properties. This conclusion can be supported by the fact that this set had mixed seeds, i.e., some seeds are from Santiago Island and some from Fogo Island. This may suggest that these seeds are more dependent on the soil composition than the environment conditions, such as temperature or humidity.

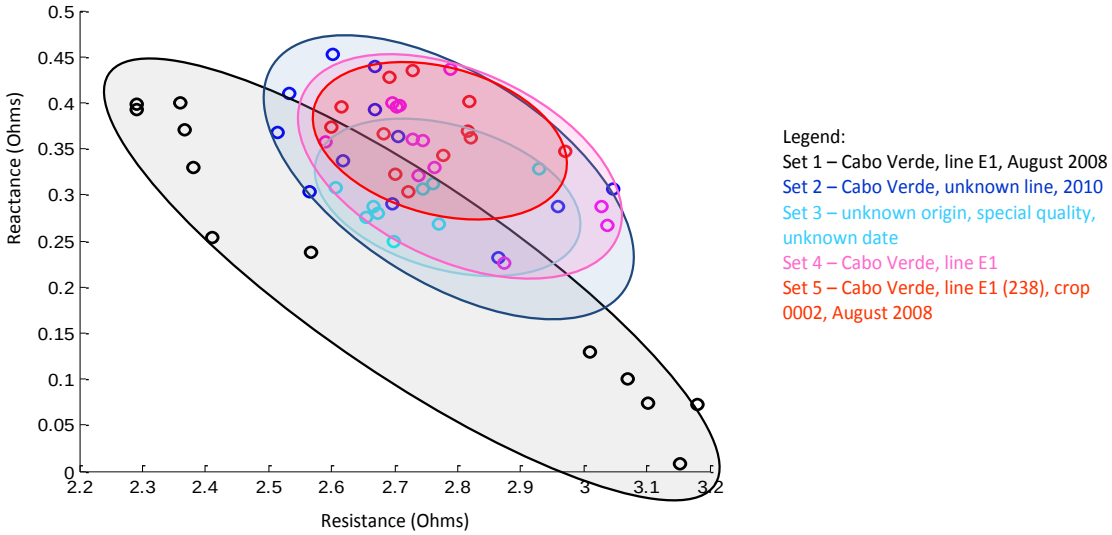

Figure 6.6: Jatropha seeds segregation based on the Z_{30k} / Z_{180k} ratio – a bioimpedance parameter.

Seeds of three different cultivars from three different harvest periods and from three different countries were tested. The main purpose was to conclude if the EIS system is able to distinguish different environmental conditions or soils compositions.

The Figure 6.7 shows a graphical dispersion of an impedance parameter for several seeds from three different countries (Cape Verde, Thailand, and India). Each plot corresponds to a different cultivar from three different countries. The seeds from India (set 3) present higher ratio deviation to the other two set regardless of the analyzed cultivar. This may suggest that the environmental conditions in India are very different when compared to Cape Verde or Thailand.

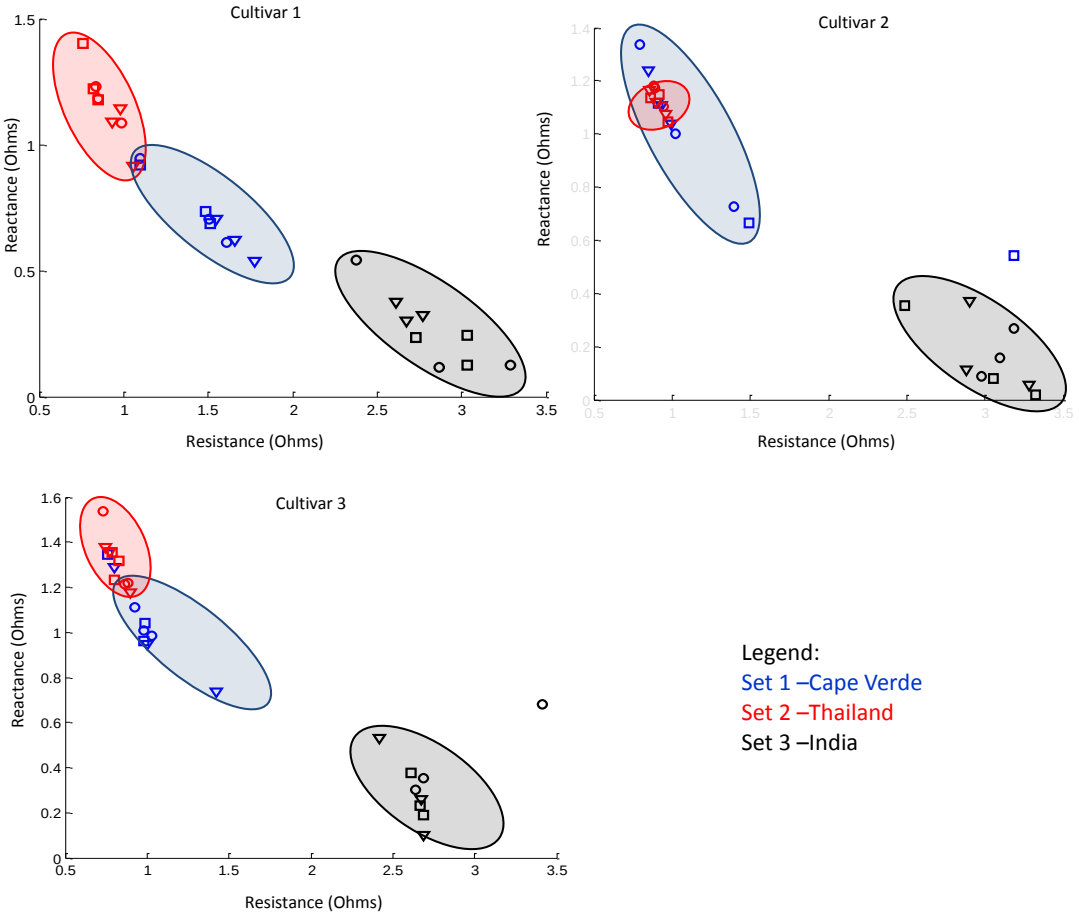

Figure 6.7: Jatropha seeds segregation based on the Z_{30k} / Z_{180k} ratio – a bioimpedance parameter. Each different marker corresponds to a different seed of the same cultivar from the same country.

6.3 Application 3

6.3.1 Motivation

Concerning the application in plant organisms, such as trees, the analysis of physiological conditions allows assessing the health state or different flowering states. For this reason the impedance method herein described could be used has an indicator of the tree healthy state. So, concrete applications in this field consist in discrimination of impedance profile between trees with and without flowers in the same environmental conditions and infer some differences after a miticides treatment.

6.3.2 Data Acquisition

The Jatropha trees used in these studies were placed in a controlled water environment at a greenhouse. To perform the EIS measurements, the electrodes were placed in the trunk of each tree, in a diametric position, and about 50cm above the soils (see Figure 6.8). Alternating current of 1 kHz to 1 MHz was passed through the biological material for impedance measurement. The acquisitions were performed every four hours and were record temperature and humidity at same time.

Figure 6.8: EIS measurement setup in the greenhouse.

For evaluated the relevance of the absence or existence of flowers in the impedance profile, two trees, one had flowers and other had not, were used. In the comparative study of healthy and unhealthy plants, once again two trees were used. One is more resistance to the mites (healthy) and the other has low resistance. For evaluated the plant behaviour after a miticide treatment the Boreal® miticide (miticide from SAPEC) was applied during the monitoring.

Figure 6.9: Healthy Jatropha tree (left) and unhealthy Jatropha tree (right).

6.3.3 Results and Discussion

For each obtained impedance spectra there were assessed several parameters, but it will only presented the results obtained for the ratio Z_{1k}/Z_{50k}.

Figure 6.10 shows a graphically dispersion of an impedance parameter for two Jatropha trees. Each plots area corresponds to a different tree. The analysis of the ratio Z_{1k}/Z_{50k} allows the conclusion that the two sets have distinct electric properties. The black set has lower impedance values when compared to the values of impedance of the green one. This conclusion can be supported by the fact that in some plants the flowering mechanism is related to a stress state. A previous analysis showed that after the flowering process the branches dried completely. So, the plant directs all its resources to survive through the flowers and then it becomes in a latent state. However, based on the potatoes study and the relationship between the water content and impedance, the achieved result is consistent to that. The flowering plant has higher impedance values and high water content.

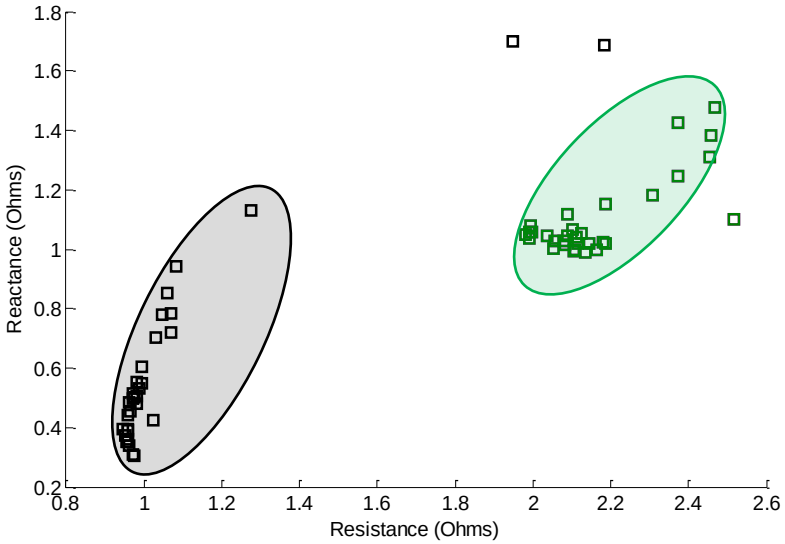

Figure 6.10: Jatropha trees segregation based on Z_{1k} / Z_{50k} ratio – a bioimpedance parameter. The black set belongs to Jatropha tree without flowers and the other to Jatropha tree with flowers.

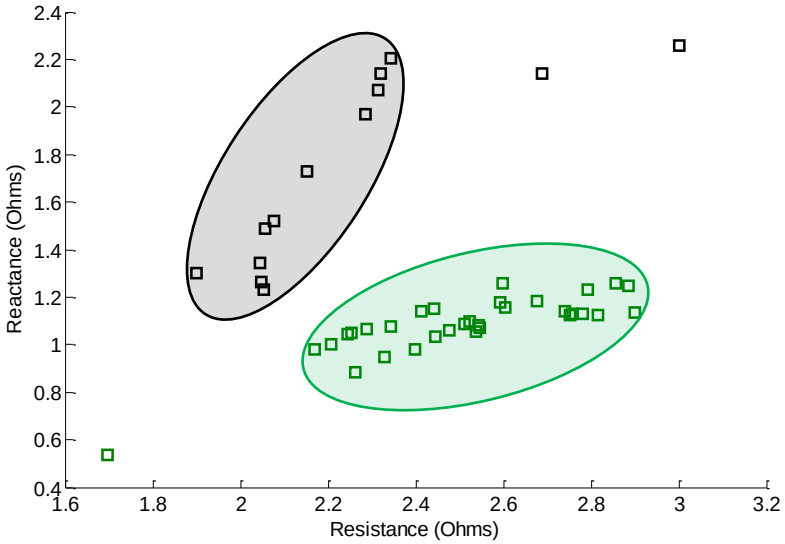

Figure 6.11: Jatropha trees segregation based on Z_{1k} / Z_{50k} ratio – a bioimpedance parameter. The black set corresponds to unhealthy plant and the green to healthy tree.

The two tested plants have different resistance to mites. Both are affected by them but on different scales, clearly observable. Although the plants are from the same

line they may have different genotype, which may have a gene that confers resistance to the mites. The analysis of the obtained results depict in Figure 6.11 shown a clear difference between the both plants and support the visible differences in each plant.

After two days from the beginning of the monitoring, both Jatrophas were treated with Boreal®. The Figure 6.12 shows a dispersion of the impedance values of the Z_{1k}/Z_{50k} parameter. As the time passed the reactance values decreases, which reflects the action of the miticides. After five days it was observed a relevant decrease of reactance and an increase of the resistance for the same parameter (see Figure 6.12).

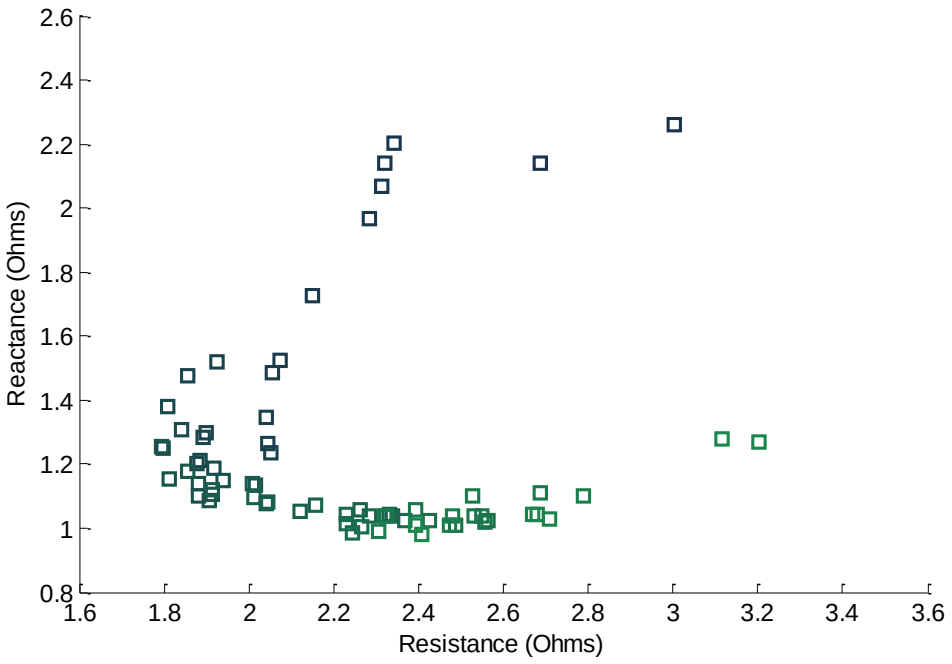

Figure 6.12: Jatropha trees Segregation based on Z_{1k} / Z_{50k} ratio – a bioimpedance parameter. Evolution of the ratio during the monitoring, before and after the miticides application. The colors graduation from black to green is in the order: first acquired data to late acquired data.

The Figure 6.13 shows that after the miticide treatment the impedance ratio of the unhealthy plant tends to the impedance values of the healthy tree. This suggests that the plant had a positively reaction to the miticide approaching to the healthy state.

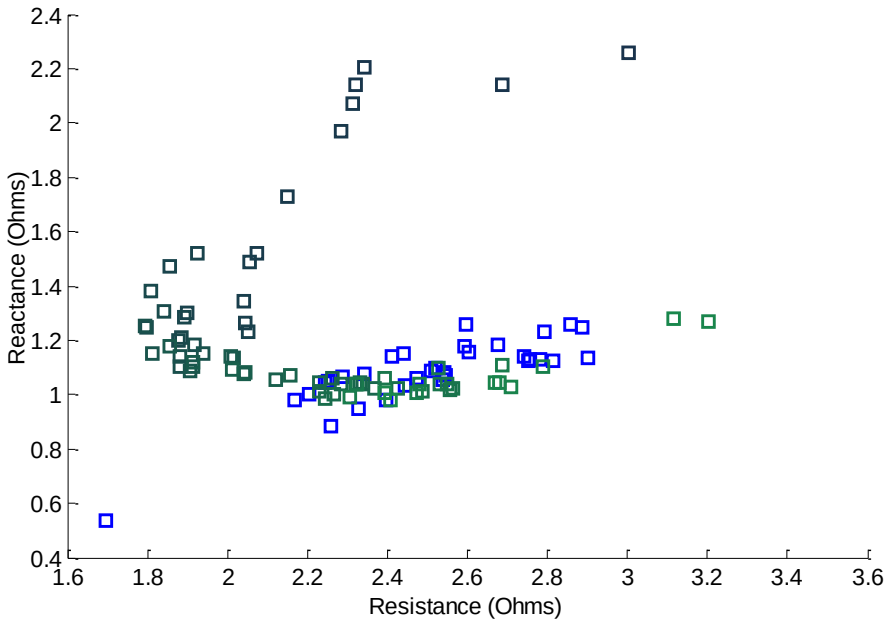

Figure 6.13: Jatropha trees Segregation based on Z_{1k} / Z_{50k} ratio – a bioimpedance parameter. Evolution of the ratio during the monitoring, before and after the miticides application (colors graduation) and data from healthy tree (blue).

6.4 Comparative Biological Test

The experimental setup 1 presented in the previous chapter was used to perform a bioimpedance measurement in a Jatropha tree. The Cole diagram obtained was compared to the one obtained with the bioimp. V.4.0 mini, as depicts in Figure 6.14.

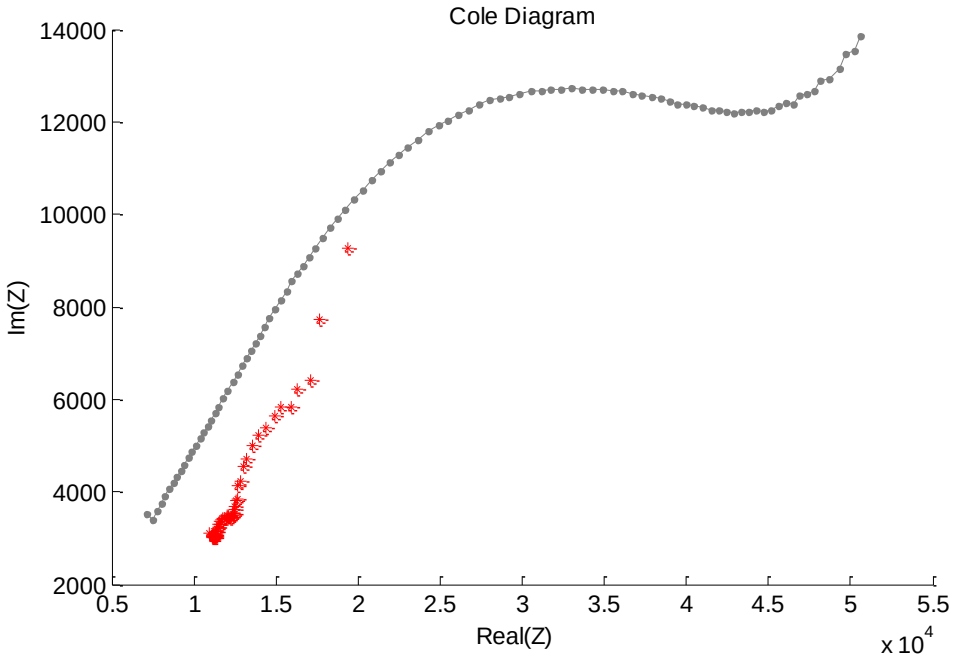

Figure 6.14: Cole-Cole Diagram for impedance data of Jatropha tree – obtained with bioimp. V.4.0 mini (grey) and experimental setup 1 (red).

The Cole Diagrams produced with the two systems are very distinct, however the distribution is similar. Since the main objective of this test was evaluated further application with the broadband excitation, it can be concluded that it is a good choice after some hardware improves.

Chapter 7

Conclusion and Future Work

7.1 Conclusion

The main objective of this project was to study a new excitation type for bioimpedance measurements. Therefore, this objective has not been totally achieved since none of the simulated signals produced consistent results with those expected. Furthermore, not all simulation results were conveniently justified. However, the study signals may be used in other applications different from the presented herein.

The experimental hardware conceived revealed the drawbacks of this technique and justified the low commercial use of it.

As presented in Chapter 3 the preliminary tests revealed a good performance of the bioimp. V.4.0 mini system. The system presents a good mean SNR for both sources and a low mean distortion. Also the implemented algorithms, as the PSD algorithm and the phase shift correction, showed quite good results analogous to the theoretical.

The biological application studies aimed at discriminating between different physiological states and verify some relation between them and bioimpedance parameters. The obtained results with the bioimp. V.4.0 mini suggest that the implemented method may constitute an innovative approach to assess physiological states, such as hydric stress or diagnosis plant diseases. Hence, the main conclusion of the developed studies is that the Z_{1k}/Z_{50k} ratio is a very helpful impedance parameter in the biological field.

7.2 Future Work

The use of Broadband signals for bioimpedance measurements described in this document should be subjected to further studies in order to answer clearly to some questions. So, it is important to conclude which is the ideal pulse waveform if the objective is to increase the Signal to Noise Ratio or which is the maximum acceptable error in magnitude and phase determination. Additionally, biological tests should be done in order to understand the utility of this type of excitation instead of the currently used.

Since this work is to be continued and based on the conclusions presented a system with this kind of signals may need an ADC with high sampling rate and with an acceptable resolution in order to introduce a tolerant error in the impedance evaluation.

Finally, it will be interesting to idealize a system with one processor (i.e., ARM) or try to implement a pipe-lining architecture. This suggestion comes against the interest of making the system independent of the PicoScope®3205A.

Appendix A

Electronic Circuits Schematics

a) Schematic of EIS system

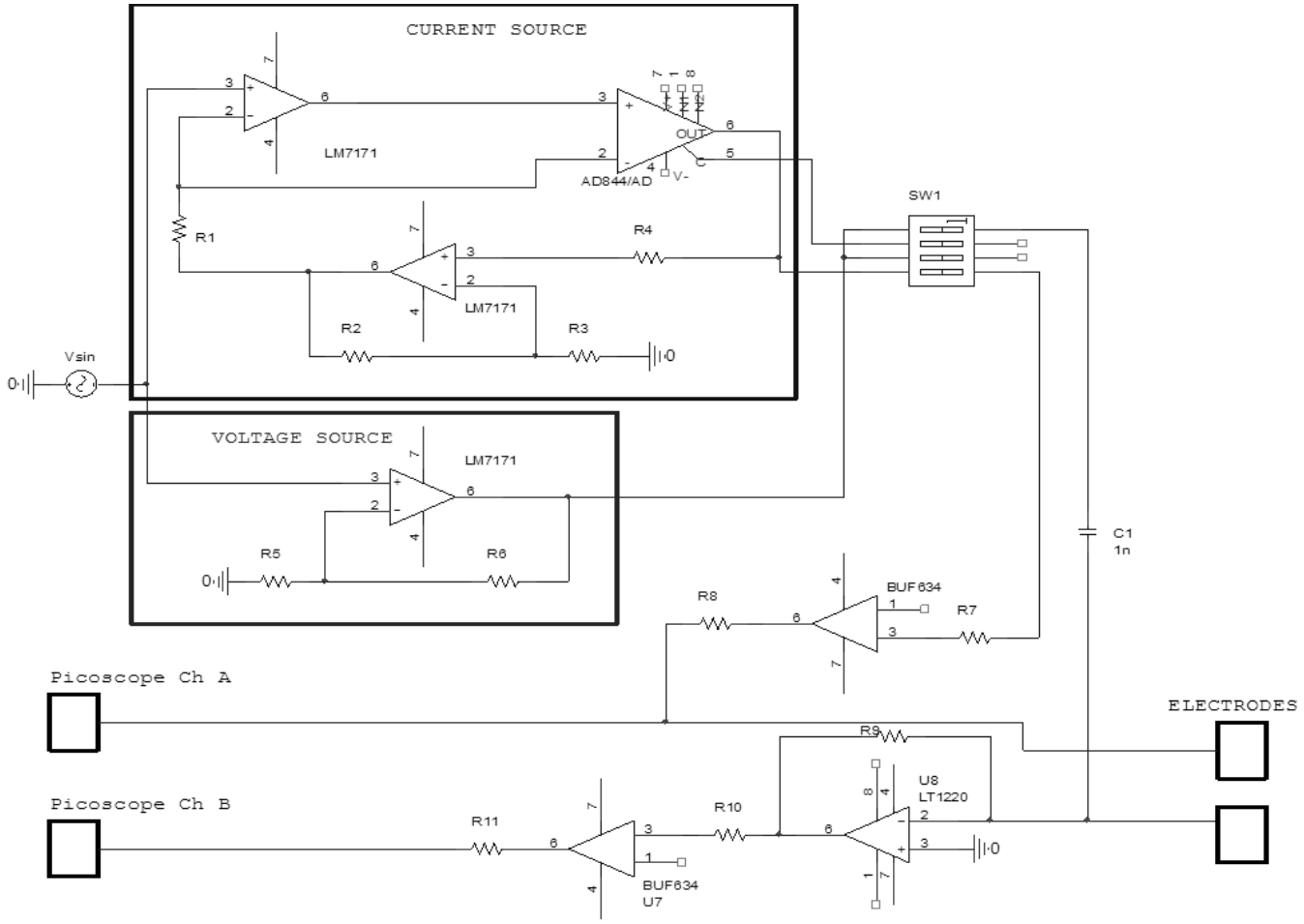

b) Schematic of pulse

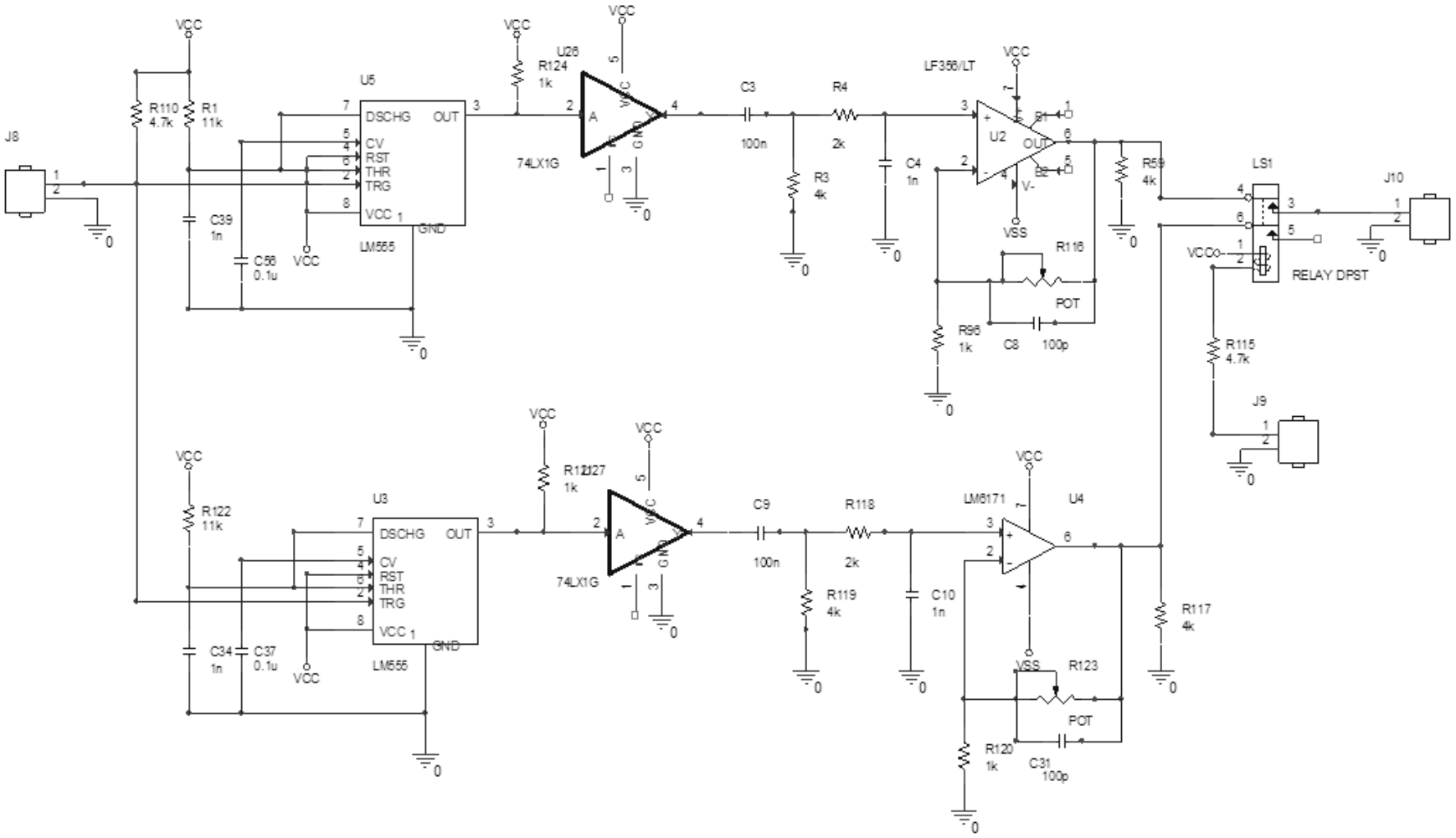

References

[1] E. B. and J. R. Macdonald, *Impedance Spectroscopy Theory, Experiment, and Applications*, Second ed. Hoboken, New Jersey: John Wiley & Sons, Inc., 2005.

[2] A. Ivorra, "Bioimpedance Monitoring for physicians: an overview," Centre Nacional de Microelectrònica Biomedical Applications Group, 2002.

[3] U. G. Kyle, I. Bosaeus, A. D. De Lorenzo, P. Deurenberg, M. Elia, J. M. Gomez, B. L. Heitmann, L. Kent-Smith, J. C. Melchior, M. Pirlich, H. Scharfetter, A. M. Schols, and C. Pichard, "Bioelectrical impedance analysis--part I: review of principles and methods," *Clinical Nutrition,* vol. 23, pp. 1226-1243, Oct 2004.

[4] E. T. Mcadams and J. Jossinet, "Tissue Impedance - a Historical Overview," *Physiological Measurement,* vol. 16, pp. 1-13, Aug 1995.

[5] G. Z. T. Repo, A. Ryyppö, and R. Rikala, "The electrical impedance spectroscopy of scot pine (Pinus sylvestris L.) shoots in relation to cold acclimation," *Journal of Experimental Botany,* vol. 51, pp. 2095-2107, 2000.

[6] J. Kourunen, T. Savolainen, A. Lehikoinen, M. Vauhkonen, and L. M. Heikkinen, "Suitability of a PXI platform for an electrical impedance tomography system," *Measurement Science and Technology,* vol. 20, pp.1-11, 2009.

[7] T. R. and A. Väinölä, "Impedance spectroscopy in frost hardiness evaluation of Rhododendron leaves," *Annals of Botany,* vol. 86, pp. 799-805, 2000.

[8] T. D. and A. Adler, "Blood Impedance Characterization from Pulsatile Measurements," presented at the IEEE CCECE/CCGEI, Ottawa, 2006.

[9] P. D. and O. Miyawaki, "Relationship between the Electrical and Rheological Properties of Potato Tuber after Various Forms of Processing," *Bioscience, Biotechnology and Biochemistry,* vol. 66, pp. 1218-1223, 2002.

[10] U. Pliquett, "Bioimpedance: A Review for Food Processing," *Food Engineering Reviews,* vol. 2, pp. 74-94, 2010.

[11] S. G. and Ø. G. Martinsen, *Bioimpedance and Bioelectrical Basics*, Second ed., 2008.

[12] F. R. H. and J. H. Maindonald, "Ripening of Nectarine Fruit," *Plant Physiology,* vol. 106, pp. 165-171, 1994.

[13] K. T. and I. Y. Hitoshi Fukuma, "Measurement of Impedance of Columnar Botanical Tissue Using the Multielectrode Method," *Electronics and Communication in Japan,* vol. 84, pp. 1593-1601, 2001.

[14] P. M. and E. Vozáry, "Effect of Mechanical Stress on Apple Impedance Parameters," *IFMBE Proceedings,* vol. 17, pp. 118-121, 2007.

[15] R. Z. y. A. Grażyna Pierzynowska-Korniak and J. Wójcik, "Electric properties of apple purée and pulpy apple juices," *European Food Research Technology,* vol. 216, pp. 385-389, 2003.

[16] S. G. and Ø. G. Martinsen, *Bioimpedance and Bioelectricity Basics*, Second ed., 2008.

[17] A. Lozano-Nieto and D. Rezywowski, "Electrical models for bioimpedance measurements," *Proceedings of the Ieee 24th Annual Northeast Bioengineering Conference,* pp. 118-119, 1998.

[18] S. G. and Ø. G. Martinsen, "Cole Electrical Impedance Model—A Critique and an Alternative," *IEEE Transactions on Biomedical Engineering,* vol. 52, pp. 132-135, 2005.

[19] M. G. Antoni Ivorra, Anna Sola, LuisPalacios, Rosa Villa, Georgina Hotter and Jordi Aguiló, "Bioimpedance dispersion width as a parameter to monitor living tissues," *Physiological Measurement,* vol. 26, pp. 1-9, 2005.

[20] L. C. Ward, T. Essex, and B. H. Cornish, "Determination of Cole parameters in multiple frequency bioelectrical impedance analysis using only the measurement of impedances," *Physiological Measurement,* vol. 27, pp. 839-850, Sep 2006.

[21] A. M.-A. and R. Pallàs-Areny, "Electrical impedance measurement using pulse excitation," presented at the 16th IMEKO TC4 Symposium Exploring New Frontiers of Instrumentation and Methods for Electrical and Electronic Measurements, Florence, Italy, 2008.

[22] M. Min, U. Pliquett, T. Nacke, A. Barthel, P. Annus, and R. Land, "Broadband excitation for short-time impedance spectroscopy," *Physiological Measurement,* vol. 29, pp. 185-192, Jun 2008.

[23] A. Technologies, *The Impedance Measurement Handbook*: Agilent Technologies Co. Ltd, 2006.

[24] H. Morel and M. Y. Jaffrin, "A bridge from bioimpedance spectroscopy to 50 kHz bioimpedance analysis: application to total body water measurements," *Physiological Measurement,* vol. 29, pp. 465-478, Jun 2008.

[25] S. H. R. and H. L. Evgenij Barsoukov, "A novel impedance spectrometer based on carrier function Laplace transform of the response to arbitrary excitation," *Journal of Electroanalytical Chemistry,* vol. 536, pp. 109-122, 2002.

[26] I. E. and Y. H. Yuri Feldman, "Time Domain Dielectric Spectroscopy Study of Biological Systems," *IEEE Transactions on Dielectrics and Electrical Insulation,* vol. 10, pp. 728-753, 2003.

[27] U. Pliquett, E. Gersing, and F. Pliquett, "Evaluation of fast time-domain based impedance measurements on biological tissue," *Biomedizinische Technik,* vol. 45, pp. 6-13, 2000.

[28] M. Rafiei-Naeini and H. McCann, "Low-noise current excitation sub-system for medical EIT," *Physiological Measurement,* vol. 29, pp. 173-184, Jun 2008.

[29] P. J. Yoo, D. H. Lee, T. I. Oh, and E. J. Woo, "Wideband bio-impedance spectroscopy using voltage source and tetra-polar electrode configuration," *Journal of Physics: Conference Series,* vol. 224, pp. 1-4, 2010.

[30] G. J. Saulnier, A. S. Ross, and N. Liu, "A high-precision voltage source for EIT," *Physiological Measurement,* vol. 27, pp. 5221-5236, May 2006.

[31] M. Rafiei-Naeini, P. Wright, and H. McCann, "Low-noise measurement for electrical impedance tomography," presented at the 13th International Conference on Electrical Bioimpedance and the 8th Conference on Electrical Impedance Tomography, 2007.

[32] G. J. Alexander S Ross, JCNewell and D Isaacson, "Current source design for electrical impedance tomography," *Physiological Measurement,* vol. 24, pp. 509-516, 2003.

[33] A. K. M. Min, R. Land, T. Parve and I. Rätsep, "Modification of Pulse Wave Signals in Electrical Bioimpedance Analyzers for Implantable Medical Devices," presented at the 26th Annual International Conference of the IEEE EMB, San Francisco, CA, USA, 2004.

[34] U. P. M. Min, T. Nacke, A. Barthel, P. Annus and R. Land, "Signals in bioimpedance measurement: different waveforms for different tasks," *IFMBE Proceedings,* vol. 17, pp. 181-184, 2007.

[35] J. H. and G. Lentka, "Method Using Square-Pulse Excitation for High-Impedance Spectroscopy of Anticorrosion Coatings," *IEEE Transactions on Intrumentation and Measurement,* vol. 60, pp. 957-964, 2011.

[36] G. S. Popkirov and R. N. Schindler, "A new impedance spectrometer for the investigation of electrochemical systems," *Review of Scientific Instruments,* vol. 63, pp. 5366-5372, 1992.

[37] R. B. E. R. Bragós, O. Casas and J. Rosell, "Characterisation of Dynamic Biologic Systems Using Multisine Based Impedance Spectroscopy," presented at the Technoloby Conference, Budapest, 2001.

[38] A. Technologies. (29-06-2012). *4294A Precision Impedance Analyzer, 40 Hz to 110 MHz.* Available: http://www.home.agilent.com/agilent/product.jspx?id=1000000858:epsg:pro&pageMode=OV&pid=1000000858:epsg:pro&lc=eng&ct=PRODUCT&cc=PT&pselect=SR.PM-Search%20Results%20-%20About%20Agilent.Overview

[39] S. Analytical. (02-07-2012). *Model 1260A Impedance / Gain-Phase Analyzer.* Available: http://www.solartronanalytical.com/Pages/1260AFRAPage.htm

[40] A. Technologies. (12-06-2012). *ENA Series Network Analyzers.* Available: http://www.home.agilent.com/agilent/product.jspx?nid=-536902639.0.00&lc=eng&cc=PT

[41] J. R. and P. R. Ramon Brag&, "A wide-band Ac-coupled current source for electrical impedance tomography," *Phisiological Measurement,* vol. 15, pp. 91-99, 1994.

[42] T. Instruments, "LM7171 Very High Speed, High Output Current, Voltage Feedback Amplifier," 2006.

[43] L. T. Corporation, "LT1220 Operational Amplifier."

[44] L. Z. Chuanhong He, 1 Bin Liu, Zheng Xu and Zhanlong Zhan, "A Digital Phase-sensitive Detector for Electrical Impedance Tomography," *IEEE Transacations on Biomedical Engineering,* 2008.

[45] Y. Y. and J. Wang, "New Tetrapolar Method for Complex Bioimpedance Measurement: Theoretical Analysis and Circuit Realization," in *Engineering in Medicine and Biology*, Shanghai, China, 2005.

[46] I. Analog Devices, "AD844, 60 MHz 2000 V/µs Monolithic Op Amp."

[47] S. Shah, A. Sharma, and M. N. Gupta, "Extraction of oil from Jatropha curcas L. seed kernels by combination of ultrasonication and aqueous enzymatic oil extraction," *Bioresource Technology,* vol. 96, pp. 121-123, Jan 2005.

[48] D. K. Garnayak, R. C. Pradhan, S. N. Naik, and N. Bhatnagar, "Moisture-dependent physical properties of jatropha seed (Jatropha curcas L.)," *Industrial Crops and Products,* vol. 27, pp. 123-129, 2008.

[49] J. Heller, *Physic nut: Jatropha curcas L.*, 1996.